Longitudinal peculiarities of planetary waves-zonal flow interaction and its role in stratosphere-troposphere dynamical coupling

Wei Ke (weike@mail.iap.ac.cn)
Institute of Atmospheric Physics, Chinese Academy of Sciences https://orcid.org/0000-0002-7616-3493

Wen Chen
Institute of Atmospheric Physics Chinese Academy of Sciences

Pavel Vargin
FSBI Central Aerological Observatory: FGBU Central'naa aerologiceskaa observatoria

Research Article

Keywords: EP flux, planetary waves, stratospheric polar vortex, stratosphere-troposphere interaction

Posted Date: March 4th, 2021

DOI: https://doi.org/10.21203/rs.3.rs-267252/v1

Longitudinal peculiarities of planetary waves-zonal flow interaction and its role in stratosphere-troposphere dynamical coupling

Ke Wei[1]*, Wen Chen[1], Pavel Vargin[2]

Affiliations

1. Center for Monsoon System Research, Institute of Atmospheric Physics, Chinese Academy of Sciences, Beijing 100029, China

2. Central Aerological Observatory of Federal Service for Hydrometeorology and Environmental Monitoring of Russia, Dolgoprudny 141700, Moscow region, Russia

Submitted to *Climate Dynamics*

February 2021

*Corresponding author address:
Ke Wei, Center for Monsoon System Research, Institute of Atmospheric Physics, Chinese Academy of Sciences, Beijing 100029, China
E-mail: weike@mail.iap.ac.cn

Abstract

The three-dimensional (3D) planetary wave analysis provides more regionalized information on stratospheric-tropospheric dynamic interactions. The upward wave flux from the troposphere to the stratosphere is maximized above north-eastern Eurasia, while the downward flux is mainly over the North America and North Atlantic (NANA) region, which is much stronger in mid and late winter. This distribution is determined by the wave-wave interaction between the different wavenumbers of planetary waves, especially between wavenumber 1 and wavenumber 2. The upward wave flux anomalies in early winter are negatively correlated with the strength of the stratospheric polar vortex (SPV). In the mid and late winter months, the strength of the SPV is positively correlated with the first mode of 3D wave flux and has a leading relationship of approximately one month. The stronger SPV corresponds to a stronger upward wave flux above northern Eurasia and stronger downward flux over the NANA region. The interannual variation in wave flux in early winter is closely associated with the Scandinavian wave train pattern. In contrast, the wave flux variation is related to the circulation anomaly corresponding to Arctic Oscillation in mid and late winter, which causes climate anomalies across the Northern Hemisphere, especially coherent temperature changes in northern Europe, eastern United States and northeastern China.

Keywords: EP flux, planetary waves, stratospheric polar vortex, stratosphere-troposphere interaction

1. Introduction

The variability of stratospheric polar vortex is considered a very important factor that can modulated the occurrence of surface weather events (Baldwin and Dunkerton, 2001; Baldwin *et al.*, 2003; Beerli and Grams, 2019; Thompson *et al.*, 2002), including occurrence frequency, intensity and regimes. Weakening of stratospheric polar vortex related to SSW events could also affect upper levels up to the ionosphere including its chemical composition (Funke *et al.*, 2017; Pedatella *et al.*, 2018). Meanwhile, the Arctic stratosphere acts as a pathway linking the extratropical surface climate to tropical El Niño–Southern Oscillation (ENSO) (e.g., Butler *et al.*, 2014; Cagnazzo and Manzini, 2009; Domeisen *et al.*, 2019; Fletcher and Cassou, 2015; Hurwitz *et al.*, 2014; Ineson and Scaife, 2009; Toniazzo and Scaife, 2006; Zhou *et al.*, 2020), Madden-Julian oscillation (MJO) (Barnes *et al.*, 2019; Song and Wu, 2020), Arctic sea ice change (e.g., De and Wu, 2019; Hell *et al.*, 2020; Kim and Son, 2020; Kim and Kim, 2020; Overland and Wang, 2019), and Indian Ocean dipole (IOD) (Hardiman et al., 2020). However, not every Arctic stratospheric polar vortex strengthening or weakening event affects the troposphere, whose state can also play an important role (Domeisen et al., 2020a).

Planetary-scale wavelike disturbances have been recognized as the dominant media in the coupling between stratosphere and troposphere and the stratospheric pathway. These planetary waves (PWs) are forced by the mechanical forcing of topography and diabatic heating caused by global distribution of land and oceans and variability of temperature contrast between continents and ocean. The condition of stratosphere can also play an important role for propagation of planetary waves (Baldwin *et al.*, 2019). The fluctuation of PWs is associated with global distribution of the momentum and heat fluxes, which can exert significant forcing on zonal-mean flow, as well as local climate anomalies. By determining the longitudinally dependent features of the general circulation, PWs engrave the climate in individual regions, e.g., altering the circumpolar flow out of zonal symmetry, creating locally intensified jets, and displacing storm tracks over the North Atlantic or North Pacific.

The Eliassen-Palm (EP) flux is a measure of the PW activity presented by Eliassen and Palm (1961). The popularity of this diagnostic wave activity flux is based on its several simple properties (Andrews and Mcintyre, 1976, 1978). First, the wave flux is parallel to the wave propagation of local group velocity for PW of small amplitudes on the meridional plane (Edmon *et al.*, 1980); second, the divergence of EP flux is related to the northward eddy quasigeostrophic potential vorticity flux and hence the conservation of wave activity density. The most important property is that the divergence of EP flux appears in the transformed Eulerian mean (TEM) equations, which explicitly associate wave forcings with zonal mean flows and is used in various studies (e.g., Chen *et al.*, 2003; Christiansen, 2001; Edmon *et al.*, 1980; Karoly, 1982). While the two-dimensional (2D) zonal-averaged EP flux can provide insight into 2D vertical and latitudinal wave propagation characteristics and wave-flow interactions in the meridional cross-section, the zonal asymmetric features are lost. Therefore, three-dimensional (3D) PW propagation was studied with the definition of 3D EP flux based on zonally uniform basic flows (Plumb, 1985), zonally varying basic flows (Takaya and Nakamura, 1997, 2001), and on the basis of primitive equations (Kinoshita and Sato, 2013; Kinoshita *et al.*, 2010). The advantage of 3D EP flux over 2D EP flux is that the zonal asymmetric feature of wave activities can be studied. For example, Plumb (1985) showed that the downward wave flux can be found in the lower stratosphere/upper troposphere above North America, while no such downward propagation feature can be revealed using the 2D EP flux. The 3D EP flux is used to study teleconnection/wave train patterns such as Pacific-North America (PNA), East Atlantic (EA) and Eurasian (EU), El Nino-Southern Oscillation (ENSO) events (Karoly *et al.*, 1989; Weare, 2010), East Pacific wave train (EPW) (Zhou et al., 2012), and Rossby wave trains contributing to the major SSW event in Antarctica in September 2002 (Peters and Vargin, 2015; Peters et al., 2007) and in Arctic in January 2003 (Peters et al., 2010). The differences in planetary wave propagation between ENSO phases were revealed using 3D Fluxes by Weare (2010). Case studies by Kodera *et al.* (2013) analyzed the vertical and zonal propagation of stratospheric planetary waves and found an association between stratospheric sudden warming (SSW) events and the subsequent

tropospheric blockings over the northern Pacific. Because the 2D EP flux is the zonal mean result of the 3D EP flux, which comprises zonally positive and negative values, the same 2D EP flux may result from a completely different wave activity distribution, which may provide important information on local climate and weather anomalies. Therefore, it is worthwhile to examine the local impact of the EP flux change.

Atmospheric internal processes are usually considered to be too chaotic to provide significant prediction skills; therefore, most climate predictions and forecasts focus on external forcings, such as SST anomalies, sea ice, and land snow cover. However, It was showed that the stratosphere exhibits extended predictability as compared to the troposphere (Domeisen et al., 2020b). Some of the stratospheric pathway influence can have delayed impacts into late winter (Hell et al., 2020; Overland and Wang, 2019; Zhang et al., 2018), even can delay to the next winter (Ren, 2012; Ren et al., 2012). Studies have shown that atmospheric internal processes can also be very important for predictions and sometimes even related to extreme events. For example, Teng et al. (2013) noted that heatwaves in the United States have a tendency to be preceded by 15-20 days by atmospheric planetary waves anomalous pattern with a wavenumber of 5, which is not necessarily linked to tropical external heating. Because wave activities are the most vigorous processes in the middle atmosphere (Domeisen et al., 2020b; Hitchcock and Simpson, 2014; Smith and Scott, 2016; Song and Robinson, 2004), the possibility of utilizing wave activities as predictors, at least for extended range weather prediction, may lead to new insights into predictability and dynamics studies.

The goal of the present paper is to investigate the longitudinal asymmetry of planetary wave propagation and its role in stratosphere-troposphere dynamical coupling. Accordingly, this paper is organized as follows. In section 2, the data and methods used in this study are described. In section 3, the 3D EP flux climatology between the stratosphere and troposphere is discussed. The EP flux is decomposed in section 4 to demonstrate the importance of wave-wave interactions between planetary waves with small wavenumbers. In section 5, the interannual variability in the 3D EP flux in the

stratosphere is discussed. In section 6, the circulation anomalies associated with the variation in EP flux in the mid and late winter are presented. Finally, a discussion of our results and conclusions are provided in section 7.

2. Data and methodology

a) Data

The primary datasets used in this study are the Japanese 55-year Reanalysis (JRA-55) (Ebita *et al.*, 2011): monthly mean temperature, geopotential height, and horizontal velocity. These data have a grid resolution of 1.25° × 1.25° from January 1958 to current, and they extend from 1000 hPa to 1 hPa with 37 vertical pressure levels. The reanalyzed surface air temperature (SAT) and meridional wind were also examined. Our analyses focused on the boreal winter. Therefore, the early winter mean was computed by averaging 2-month periods of November and December (ND) during each year, and the mid and late winter mean was obtained by averaging the 3 months of January, February, and March (JFM) during each year. We assume that our results will not change when other reanalysis data is used due to similarities of all reanalysis in representation of large scale dynamical processes in the stratosphere (Ayarzagüena et al., 2019). Meanwhile, the monthly Arctic Oscillation and Pacific Decadal Oscillation index data was adopted from the Climate Prediction Center (https://www.cpc.ncep.noaa.gov/). The Scandinavian Pattern index was obtained using rotated empirical orthogonal function following Liu *et al.* (2014). We also used the Extended Reconstructed Sea Surface Temperature (ERSST, version 5) dataset (Huang *et al.*, 2017) provided by the NOAA/OAR/ESRL PSD, Boulder, Colorado, USA, from their web site at https://www.esrl.noaa.gov/psd/.

b) 3D EP fluxes

The 3D EP fluxes were calculated as a diagnostic tool to measure the wave activity propagation, which can be expressed in the log-pressure coordinates on a sphere (Plumb, 1985) as follows:

$$
\begin{aligned}
F_s &= p\cos\phi \begin{pmatrix} \frac{1}{2a^2\cos^2\phi}\left[\left(\frac{\partial\psi'}{\partial\lambda}\right)^2 - \psi'\frac{\partial^2\psi'}{\partial\lambda^2}\right] \\ \frac{1}{2a^2\cos\phi}\left[\frac{\partial\psi'}{\partial\lambda}\frac{\partial\psi'}{\partial\phi} - \psi'\frac{\partial^2\psi'}{\partial\lambda\partial\phi}\right] \\ \frac{2\Omega^2\sin^2\phi}{N^2 a\cos\phi}\left[\frac{\partial\psi'}{\partial\lambda}\frac{\partial\psi'}{\partial z} - \psi'\frac{\partial^2\psi'}{\partial\lambda\partial z}\right] \end{pmatrix} \\
&= p\cos\phi \begin{pmatrix} \frac{1}{2a^2\cos^2\phi}\left[2\left(\frac{\partial\psi'}{\partial\lambda}\right)^2 - \frac{\partial}{\partial\lambda}\left(\psi'\frac{\partial\psi'}{\partial\lambda}\right)\right] \\ \frac{1}{2a^2\cos\phi}\left[2\frac{\partial\psi'}{\partial\lambda}\frac{\partial\psi'}{\partial\phi} - \frac{\partial}{\partial\lambda}\left(\psi'\frac{\partial\psi'}{\partial\phi}\right)\right] \\ \frac{2\Omega^2\sin^2\phi}{N^2 a\cos\phi}\left[2\frac{\partial\psi'}{\partial\lambda}\frac{\partial\psi'}{\partial z} - \frac{\partial}{\partial\lambda}\left(\psi'\frac{\partial\psi'}{\partial z}\right)\right] \end{pmatrix}
\end{aligned}
\tag{1}
$$

where a, Ω, λ, φ, N, H are the Earth's radius, the Earth's rotation rate, longitude, latitude, buoyancy frequency, and constant scale height, respectively. In the above expression, p = pressure/1000 hPa, z = $-H\ ln\ p$, and the vector $\boldsymbol{F}_s$ is the 3D stationary wave flux of (hereafter, the 3D EP flux) under the quasigeostrophic approximation. ψ' is the streamfunction with the small perturbation to its zonal mean. The Plumb flux are widely used as the vectors are proportional to the group velocity of a planetary wave packet under the assumption of slow variability of the basic state (so-called WKB limit), indicating the direction of the wave flux propagation.

To obtain the basic modes of the 3D EP flux interannual variability, an empirical orthogonal function (EOF) analysis was applied in this study, which was conducted by constructing an area-weighted covariance matrix. The gridded data of the vertical component (EPz) of EP flux were weighted by the square root of the cosine of latitude

to ensure that equal areas were afforded equal weight in the analyses. We regressed the wintertime unweighted anomaly fields upon the standardized principal component (PC) time series and plotted the resulting regression coefficients. Thus, the values in the regression maps corresponded to anomaly values that were associated with one standard deviation anomaly in the PC time series. The linear correlation coefficients were calculated between time series. A two-tailed Student's *t*-test was employed to test the significance of the results.

c) The 3D EP flux decomposition

The three-dimensional wave activity flux by Plumb (1985) can be further decomposed into contribution components of each wavenumber and wave-wave interaction.

If we define $\psi' = \sum \psi_i' = \sum \Psi_i \sin\Theta_i$, and $\psi^{*\prime} = \sum \psi_i{}^{*\prime} = \sum \Psi_i \cos\Theta_i$, in which $\Theta_i = k_i\lambda + l_i\phi + m_i z + \theta_i$, and i is the wavenumber, we obtain the following equations:

$$
\begin{aligned}
F_x &= p\cos\phi \frac{1}{2a^2\cos^2\phi}\left[\left(\frac{\partial\psi'}{\partial\lambda}\right)^2 - \psi'\frac{\partial^2\psi'}{\partial\lambda^2}\right] \\
&= p\cos\phi \frac{1}{2a^2\cos^2\phi}\left[\left(\sum\frac{\partial\psi_i'}{\partial\lambda}\right)^2 - \sum\psi_i'\sum\frac{\partial^2\psi_i'}{\partial\lambda^2}\right] \\
&= p\cos\phi \frac{1}{2r^2\cos^2\phi}\left[\sum\left(\left(\frac{\partial\psi_i'}{\partial\lambda}\right)^2 - \psi_i'\frac{\partial^2\psi_i'}{\partial\lambda^2}\right) + \sum\left(\frac{\partial\psi_i'}{\partial\lambda}\frac{\partial\psi_j'}{\partial\lambda} - \psi_i'\frac{\partial^2\psi_j'}{\partial\lambda^2}\right)\right] \\
&= p\cos\phi \frac{1}{2a^2\cos^2\phi}\left[\sum F_{xi} + \sum F_{xij}\right]
\end{aligned}
\qquad (2)
$$

in which $F_{xi} = \left(\frac{\partial\psi_i'}{\partial\lambda}\right)^2 - \psi_i'\frac{\partial^2\psi_i'}{\partial\lambda^2}$, and $F_{xij} = \frac{\partial\psi_i'}{\partial\lambda}\frac{\partial\psi_j'}{\partial\lambda} - \psi_i'\frac{\partial^2\psi_j'}{\partial\lambda^2}$, where F_{xi} denotes the wave activity in the x direction due to the wavenumber i, and F_{xij} denotes the wave activity caused by the wave interaction between the wavenumber i and j, i.e., action of wavenumber i on wavenumber j.

Similarly,

$$
\begin{aligned}
F_y &= p\cos\phi\frac{1}{2a^2\cos\phi}\left[\frac{\partial\psi'}{\partial\lambda}\frac{\partial\psi'}{\partial\phi}-\psi'\frac{\partial^2\psi'}{\partial\lambda\partial\phi}\right] \\
&= p\cos\phi\frac{1}{2r^2\cos\phi}\left[\sum\frac{\partial\psi_i'}{\partial\lambda}\sum\frac{\partial\psi_i'}{\partial\phi}-\sum\psi_i'\sum\frac{\partial^2\psi_i'}{\partial\lambda\partial\phi}\right] \\
&= p\cos\phi\frac{1}{2a^2\cos\phi}\left[\sum\left(\frac{\partial\psi_i'}{\partial\lambda}\frac{\partial\psi_i'}{\partial\phi}-\psi_i'\frac{\partial^2\psi_i'}{\partial\lambda\partial\phi}\right)+\sum\left(\frac{\partial\psi_i'}{\partial\lambda}\frac{\partial\psi_j'}{\partial\phi}-\psi_i'\frac{\partial^2\psi_j'}{\partial\lambda\partial\phi}\right)\right] \\
&= p\cos\phi\frac{1}{2a^2\cos\phi}\left[\sum F_{yi}+\sum F_{yij}\right]
\end{aligned}
\tag{3}
$$

in which $F_{yi}=\frac{\partial\psi_i'}{\partial\lambda}\frac{\partial\psi_i'}{\partial\phi}-\psi_i'\frac{\partial^2\psi_i'}{\partial\lambda\partial\phi}$, and $F_{yij}=\frac{\partial\psi_i'}{\partial\lambda}\frac{\partial\psi_j'}{\partial\phi}-\psi_i'\frac{\partial^2\psi_j'}{\partial\lambda\partial\phi}$, where F_{yi} denotes the wave activity in the *y* direction due to the wavenumber *i*, and F_{yij} denotes the wave activity caused by the action of wavenumber *i* on wavenumber *j*.

$$
\begin{aligned}
F_z &= p\cos\phi\frac{2\Omega^2\sin^2\phi}{N^2a\cos\phi}\left[\frac{\partial\psi'}{\partial\lambda}\frac{\partial\psi'}{\partial z}-\psi'\frac{\partial^2\psi'}{\partial\lambda\partial z}\right] \\
&= p\cos\phi\frac{2\Omega^2\sin^2\phi}{N^2a\cos\phi}\left[\sum\frac{\partial\psi_i'}{\partial\lambda}\sum\frac{\partial\psi_i'}{\partial z}-\sum\psi_i'\frac{\partial^2\psi_i'}{\partial\lambda\partial z}\right] \\
&= p\cos\phi\frac{2\Omega^2\sin^2\phi}{N^2r\cos\phi}\left[\sum\left(\frac{\partial\psi_i'}{\partial\lambda}\frac{\partial\psi_i'}{\partial z}-\psi_i'\frac{\partial^2\psi_i'}{\partial\lambda\partial z}\right)+\sum\left(\frac{\partial\psi_i'}{\partial\lambda}\frac{\partial\psi_j'}{\partial z}-\psi_i'\frac{\partial^2\psi_j'}{\partial\lambda\partial z}\right)\right] \\
&= p\cos\phi\frac{2\Omega^2\sin^2\phi}{N^2a\cos\phi}\left[\sum F_{zi}+\sum F_{zij}\right]
\end{aligned}
$$

(4)

in which $F_{zi}=\frac{\partial\psi_i'}{\partial\lambda}\frac{\partial\psi_i'}{\partial z}-\psi_i'\frac{\partial^2\psi_i'}{\partial\lambda\partial z}$, and $F_{zij}=\frac{\partial\psi_i'}{\partial\lambda}\frac{\partial\psi_j'}{\partial z}-\psi_i'\frac{\partial^2\psi_i'}{\partial\lambda\partial z}$, where F_{zi} denotes the wave activity in the vertical direction due to the wavenumber *i*, and F_{zij} denotes the wave activity caused by action of wavenumber *i* on wavenumber *j*.

the zonal average:

$$\overline{F_x} = \sum \overline{F_{xi}} = p\cos\phi \frac{1}{2r^2\cos^2\phi} \sum k_i^2 \Psi_i^2$$
$$\overline{F_y} = \sum \overline{F_{yi}} = p\cos\phi \frac{1}{2r^2\cos\phi} \sum k_i l_i \Psi_i^2 \quad (5)$$
$$\overline{F_z} = \sum \overline{F_{zi}} = p\cos\phi \frac{2\Omega^2 \sin^2\phi}{N^2 r\cos\phi} \sum k_i m_i \Psi_i^2$$

Therefore, the zonal mean wave flux comes from the combination/sum of wave activities from each wavenumber, while the zonal asymmetric component of the wave flux comes from the interaction between waves.

3. The 3D EP flux between the stratosphere and troposphere

The planetary EP flux is prohibited in the summer season by the easterly in the stratosphere. When the stratosphere westerly and polar vortex are gradually restored in autumn, planetary waves propagate upward, and the polar vortex is prone to distortions by the wave activities from the troposphere. The 3D EP flux at 30 hPa (~24 km, middle stratosphere) in the winter months is demonstrated in Figure 1. The upward EP flux (EPz) is very weak in October (Figure 1a), favoring the strengthening and construction of the SPV. From November inside the polar night darkness, a strong radiative cooling greater than 8°K day^{-1}(Kiehl and Solomon, 1986) inside the polar region drives the Arctic stratosphere to an extremely cold state. The dynamic energy fluxes resulting mainly from planetary waves act as the key processes driving the circulation out of radiative equilibrium and maintaining the temperature observed in the stratosphere. The other important process is gravity waves propagated though stratosphere although their influence on circulation is more pronounced in the upper stratosphere and mesosphere (Ern *et al.*, 2016). The upward EP flux intensifies during winter (Figure 1b and 1c) and reaches its maximum in January (Figure 1d), centered above the far end of the northeast Eurasia continent. The horizontal wave flux (EPx and EPy) shows a circumpolar propagation, which starts above Europe and ends above Greenland and the northern

Atlantic. Equatorward wave fluxes are mainly manifested around Europe and the east Pacific-North America section, as demonstrated by Plumb (1985) and other studies (e.g., Randel and Williamson, 1990; Yang and Gutowski, 1994; Zhou *et al.*, 2012). Interestingly, there are downward EPz values above the Baffin Bay, Greenland, and the northwest Atlantic, which are usually absent in the 2D EP flux analysis. Therefore, the total 2D EP wave flux entering the stratosphere is the net addition of the upward and downward EP fluxes above different regions. The downward wave flux is nearly absent in November, very weak in December, strong in January and February, and fading in March, confirming the results of (Zyulyaeva and Jadin, 2009). The upward EPz is responsible for the source of the eddy energy from the troposphere, while the downward EPz implies the eddy energy sink from the stratosphere. It should be noted that the wave fluxes, both vertical and horizontal, are very weak and almost absent over East Atlantic region, just like there is a barrier for wave propagation.

The longitude-height section of EPz and EPx in Figure 2 exhibits the seasonal evolution of wave activities during the winter season at 65 °N. The downward EP flux is strongest in January, both in strength and active domain. Although the maximum value of the downward flux is comparable to that of the upward flux, the domain and strength of the downward flux are still less than those of the upward flux. The features of Plumb flux remain if wider latitudinal belt for instance 50-70 °N is used. In the barrier region of 0-30°W, the wave fluxes are very weak in the domain of stratosphere. This wave structure of downward and upward wave fluxes was called a stratospheric bridge by Kodera *et al.* (2008) using case studies and by Zyulyaeva and Jadin (2009) using long-term data analysis. Zyulyaeva and Jadin (2009) and Jadin (2011) concluded that the stratospheric bridge is formed in January-February, which plays a significant role in the stratospheric circulation in late winter because it is responsible for the exchange of the eddy energy between the troposphere and stratosphere .

Whether the wave propagates upward or downward in the atmosphere is determined by the vertical tilting of the wave structure. When the trough/ridge tilt westward with

height, the EPz flux is upward, while the EPz flux is downward when the trough/ridge tilt eastward with height. As the filtering effect of the stratospheric jet stream (Charney and Drazin, 1961), only waves with small wave numbers (waves 1 and 2) can propagate into the stratosphere, while other large wave number (small scale) components are trapped in the troposphere. PW of wavenumber 1 (PW1) can reach the upper stratosphere and have the largest amplitude in that area (Figure 3a); however, the amplitude of PW of wavenumber 2 (PW2) has the largest value in the mid and lower stratosphere (Figure 3b). In the stratosphere, the PW1 pattern manifests itself as a trough over the northern Atlantic and a ridge over the northern Pacific, while in the troposphere, the PW2 structure is the most dominant, with two troughs over the coastal region of East Asia and northeast America and two ridges over the North Pacific and Western Europe. Therefore, combining the structure of PW1 and PW2, the tropospheric East Asian trough extends upward and westward and integrates into the stratospheric northern Atlantic trough (Figure 3c). In comparison, the tropospheric northeast American trough extends upward and eastward until it merges into the stratospheric northern Atlantic trough (Figure 5c). Therefore, the combination of wave 1 in the stratosphere and wave 2 in the troposphere favors the upward wave flux over the Eurasian continent and downward wave flux over northeast America and the northern Atlantic.

The winter (DJF) 3D EP flux decomposition at 65 °N (Figure 4) indicates that the zonal symmetric components (Figure 4b) have an upward flux throughout all longitudes, which is caused by the sum of wave activities from each wavenumber, while the asymmetric part (Figure 4c) comes from the interaction between waves, which have upward fluxes over most of the eastern hemisphere, centered over the far end of the northeast Eurasia continent and have a downward flux over the western hemisphere, centered over North America in the upper troposphere and lower stratosphere (200-100 hPa) and tilting to North Atlantic in the middle and upper stratosphere. Therefore, to investigate the geographical feature and influence of the planetary wave flux, it is necessary to analyze the wave-wave interactions.

The asymmetric part is decomposed according to the interaction between each wave. For example, EP(2,1) represents the action of PW2 on PW1, while EP(1,2) represents the action of PW1 on PW2. The decomposition results show that the main contribution of the asymmetric part comes from EP(2,1), that is, the action of wavenumber 2 on wavenumber 1 (Figure 4d), which has an upward flux mainly over the eastern hemisphere and downward flux over the western hemisphere from the upper troposphere upward to the upper stratosphere. The contribution from EP(1,2) is small, and the centers are ~90° to the east of the centers of EP(2,1) at 50 hPa. The contribution from EP(3,1) (Figure 4e) is relatively small and mainly concentrated in the lower levels, which help to depict some minor details, such as the relatively small value between 60°E-90°E and the negative center between 120°W-90°W at 200 hPa. The contributions of other wave interactions are very small (Figure 4 g-i). Therefore, if we want to study the variability of the zonal-mean circulation change in the stratosphere-troposphere system, we may need to pay attention to sum of wave activities from each wave numbers. However, if we want to understand the regional change characteristics of the process of stratospheric-tropospheric interaction, more attention should be focused on the interaction between waves, especially the interaction between wavenumber 1 and 2.

4. The dominant mode of the 3D EP flux

The wave flux between the troposphere and stratosphere shows large interannual variations, which are considered to be the main cause of the strength of the SPV and are the key processes corresponding to the influence of the Holton-Tan Oscillation (Anstey and Shepherd, 2014; Anstey *et al.*, 2010; Baldwin *et al.*, 2001), Pacific Decadal Oscillation (Jadin *et al.*, 2010), ENSO (Wei *et al.*, 2007), North Pacific SST anomalies (Hurwitz *et al.*, 2012), Siberian snow cover anomalies in autumn (Cohen *et al.*, 2014), and the solar cycle (Kodera, 2006; Kodera and Kuroda, 2002). The dominant interannual variation in the 3D EP flux in the stratosphere can be investigated with an EOF analysis, and the results are shown in Figure 5, which are the first EOF (EOF1) of EPz at 30 hPa for the winter months from October to March. In the early winter months,

the contributions of EOF1 to the total variance were 45.4% in Oct, 52.1% in November, and 44.4% in December. The dominant mode is featured with a positive EPz over northeastern Eurasia, which intensifies from October to December. These centers are approximately in the same regions as the climatology (Figure 1a-c). Therefore, the interannual variations in the 3D EP flux in early winter manifest as the strength change in the upward wave flux, which will influence the strength of the circumpolar flow and polar vortex.

In January and February (Figure 5 d and e), the dominant mode of 3D EP flux shows positive EPz anomalies with the maximum over north-eastern Eurasia, and negative EPz anomalies over Canada, southern Greenland, and northern Atlantic, in approximately the same regions as the upward and downward propagation of planetary waves in their climatology (Figure 1 d and e). The contributions of EOF1 to the total variance are larger (35.5% and 36.7%) than those of the second EOF (20.9% and 20.5%, figures not shown). The amplitude of the downward wave flux is comparable to that of the upward flux in January and February. Therefore, the most prominent feature of the first EOF spatial pattern is the dipole-like structure in January and February, not in the early winter months of ND.

The stratospheric circulation variability in the high latitudes is characterized by changes in the polar jet that has a nearly annular mode (Kuroda and Kodera, 1999). We calculated the lagging/leading correlations of the January zonal-mean zonal wind (65ºN) at 30 hPa with the EPz at 65ºN from October to April, as shown in Figure 6. During December (Figure 6a), the strength of the January polar jet is associated with a decrease in EPz over the whole longitude, and negative correlation can also be observed in the preceding November, implying that the acceleration (deceleration) of the mid-winter polar jet in January is associated with the weakening (strengthening) of the planetary wave penetration from the troposphere to the stratosphere over northern Eurasia in the preceding month, indicating that the anomalies of the wave penetration into the stratosphere have some kind of accumulative effect in early winter. When the upward

wave flux is weaker than usual in the late autumn and early winter, a stronger polar night jet is generated in mid-winter. Otherwise, when the upward wave flux is stronger than usual in late autumn and the early winter months, a weaker polar vortex or a mid-winter SSW is generated in January.

However, this relationship is absent in the mid and late winter months. The January polar jet strength is associated with an EPz dipole pattern, shown as a positive correlation over northeast Asia and a negative correlation over North America and the North Atlantic (NANA) region. This pattern lasted from January to the following February and March. Notably, the dipole correlation pattern between the mid-winter (January) polar jet strength and EPz, with positive and negative correlation centers at approximately 180º and 30ºW, persists through JFM, indicating a lagged response of the wave activities to the mid-winter polar vortex strength. Therefore, two regimes in the forcing of the upward and downward EPz fluxes on the stratospheric circulation can be identified in January-February. 1) The cold polar vortex regime: when the polar vortex is stronger, the downward EPz flux is large over the North Atlantic, a significant part of the eddy energy accumulated in the early winter months of ND can be transferred to the troposphere over the North Atlantic. 2) The warm polar vortex regime: when a warm polar vortex is observed in mid winter, the downward eddy energy over the North Atlantic is small, then the exchange of the eddy energy from the stratosphere to the troposphere is blocked.

The interaction between the vertically propagating wave activities and the polar vortex strength can also be explored with the leading/lagged correlation coefficient between the polar vortex jet and the first principle component of EPz in the stratosphere (Table 1). The correlation coefficients are mostly negative in the early winter months (ND), while they are mostly positive in the mid and late winter months (JFM). The results confirm the correlation of Zyulyaeva and Jadin (2009), which made a lead-lag analysis between the leading EOF PC for 3D EP flux and for zonal wind at 30 hPa based on NCEP/NCAR reanalysis data. The contemporaneous correlation between the January

jet strength and the dominant mode of EPz is 0.156, which is essentially less by its absolute value than that between the January Jet strength and EPz PC1 in December (-0.484). This can imply that the mid-winter strengthening (weakening) of the SPV is more associated with the decreased (increased) planetary wave penetration from the troposphere to the stratosphere over northern Eurasia in the preceding month. However, the relationship changes in the late winter months. The correlation becomes positive, and the strength of the polar vortex in the preceding month determines the wave properties in the next month. For example, the contemporaneous correlation coefficient between the polar jet and EPz PC1 in January is 0.156, while it is 0.305 between the January polar jet and February EPz PC1. The contemporaneous correlation coefficient between the polar jet and EPz PC1 in February is 0.208, while it is 0.359 between the February polar jet and March EPz PC1.

Wave decomposition shows that the negative correlation of early winter EPz with January polar jet is mainly caused by the EPz sum of wave activities from each wavenumber (Figure 6b). While the dipole correlation pattern between EPz in mid and late winter and the mid-winter (January) polar jet strength is caused by the wave-wave interaction component (Figure 6c), which is dominated by the EPz from the action of PW2 on PW1 (Figure 6d). Therefore, the linkage between stratosphere polar vortex and wave activities can be divided into two parts.

1) the interaction between the strength of polar vortex and the wave amplitude change: when PW amplitude decreases in early winter, it leads to a stronger polar vortex. While in mid and late winter, the strength of polar vortex in January is unrelated to the PW amplitude change (Figure 6b).

2) the modulation of the wave-wave by the strength of polar vortex. The polar vortex can have a significant influence on the wave-wave interaction, especially the action of PW2 on PW1, mainly during the mid and late winter.

In December, a stronger mid-winter polar vortex is associated with weaker PW1 (Figure

7a). Both the ridge and trough of PW1 are weaker than the climatology, and the anomaly follows the west-tilted structure of PW1. In January, however, a stronger mid-winter polar vortex is associated with stronger PW1 in the upper stratosphere (Figure 7c) and stronger PW2 from the upper troposphere to the upper stratosphere (Figure 7d). This is contrary to the conventional understanding that stronger polar vortex is caused by weaker PW activities. The anomaly centers of PW1 locates about 30 degrees to the east of the climatological ridge and trough centers at the upper stratosphere (1hPa). While the anomaly centers shift about 90 degrees to the west of the climatological ridge and trough centers at the middle stratosphere (30hPa). The anomaly centers shift further westward at the low stratosphere (100hPa), almost 180 degrees phase difference with the climatology, leading to weaker PW1 at this level. The vertical structure of the PW1 is modified by the eastward tilting of the PW1 anomaly, which together with the amplified PW2, favors downward wave flux propagation. In February, the January stronger polar vortex is associated with east-tilted anomaly of both PW1 and PW2 in the upper stratosphere (Figure 7e and 7f). In the upper stratosphere above ~7hPa, the PW1 strengthens and shifts eastward. While in the middle stratosphere, the PW1 strengthens and shifts westward. The PW2 strengthens throughout the troposphere and stratosphere, and shifts eastward in the upper stratosphere. This creates ideal conditions for a stronger wave bridge in the stratosphere.

The differences between the early winter and late winter can be understood as the dynamic coupling differences between these two periods. The sink of the eddy energy over the North Atlantic may be a key process in the wave-zonal flow interaction in January-February in contrast with that in early winter. In the early winter months, the dominant 3D EP flux mode (positive phase) is associated with a weakened polar jet (Figure 8c), while the dominant EP flux mode is associated with a stronger SPV in late winter (Figure 8f). During the early winter, when the polar vortex is building up, and the polar jet is accelerating, the dynamic forcing of the planetary wave can influence the strength of the polar vortex, which is the conventional understanding between the upward wave flux and zonal flow, i.e., stronger upward wave flux leading to a weaker

zonal flow. In the late winter, the conventional perspective is reversed with a stronger wave coupling associated with the stronger westerly jet. The positive correlation between the PC 1 of EPz and the polar jet can be understood as the response of wave activities to the circulation change in the stratosphere. When mid-winter stratospheric warming appears and lasts for approximately one month, the weak zonal flow (or easterly during major warming events) creates an unfavorable configuration for the wave activities in the stratosphere, which causes a weak upward EPz flux over the north of Eurasian continent and North Pacific (ECNP) and weak downward EPz flux over the NANA region. Wei and Chen (2012) analyzed the association between the northern hemisphere stratosphere polar vortex extremes in February with the wave flux in the lower stratosphere. The extremely warm polar vortex in February follows the mid-winter major warming in January, featuring a very weak (near zero) downward EP flux over the NANA region. The extremely strong polar vortex features a strong downward EP flux over the NANA region.

5. The association with lower-level circulation and sea surface temperature

In the early winter months, corresponding to stronger wave fluxes into the stratosphere, the circulation distribution shows a wave train in the low troposphere (Figure 9a), with a positive geopotential height anomaly over the central North Atlantic, a negative anomaly over Britain, a positive anomaly over northern Europe, and a negative anomaly over Lake Baikal and eastern Siberia. The temperature anomalies show negative centers over Britain and western Europe, Lake Baikal and eastern Siberia, and positive values over eastern and northern Europe, northeastern Canada and northern part of North America. This kind of distribution is nearly identical to the wave train of the Scandinavian Pattern (Bueh and Nakamura, 2007; Liu *et al.*, 2014). The correlation coefficient between the first wave flux PC and the Scandinavian Pattern index is -0.73

(p=0.0001) in early winter, suggesting that the Scandinavian wave train pattern in the early winter is conducive to the propagation of planetary waves to the stratosphere, thus weakening the SPV in midwinter. Wave decomposition of the circulation into planetary waves (wave 1, 2 and 3) and synoptical waves (wave 4 and above) shows that the low-level wave train is related to both planetary waves (Figure 9c) and synoptical waves (Figure 9e).

Although previous studies revealed that the Scandinavian Pattern is associated with SST anomaly over the mid-latitude northwestern Atlantic (Bueh and Nakamura, 2007) or over the tropical and southern Indian Ocean (Liu *et al.*, 2014), our regression/correlation (Figure 10a) shows that the strongest and significant signals are above the center North Pacific. And the correlation coefficient between EOF PC1 of EPz and Pacific Decadal Oscillation index is 0.33 (p=0.03), indicating a remote influence from the North Pacific via Rossby-wave propagation. This is consistent with the model results of Hurwitz *et al.* (2012) who revealed a lagged negative correlation between SST in Northern Pacific in January-February with March lower stratospheric polar cap temperature: positive SST anomalies in Northern Pacific are followed by stronger stratospheric polar vortex.

During the mid and late winter months (January to March, Figure 9b), the positive EPz EOF1 phase is associated with negative geopotential height anomalies at 850 hPa over the Arctic and Greenland regions and positive anomalies at 850 hPa in the midlatitude regions of the central North Atlantic, the Bering Sea and the Aleutian Islands in the North Pacific. Accordingly, positive temperature anomalies occur over southeastern North America, western and northern Europe, and Northeast Asia, while negative temperature anomalies mainly occur over the Baffin Bay, Alaska, northern North America, Caspian Sea, Western Asia, and North Africa.

This kind of distribution of temperature and geopotential height anomalies is very close to the positive phase of Arctic Oscillation (Thompson and Wallace, 2000) and is consistent with the low-level circulation pattern corresponding to a stronger SPV (Chen

and Wei, 2009). The correlation coefficient between the first wave flux PC and the AO index is 0.33 (p=0.02) in late winter. Wave decomposition shows that the low-level circulation anomaly is mainly related to planetary waves (Figure 9d), while the synoptical wave component is very small (Figure 9f). The sea surface temperature anomalies associated with the wave flux (Figure 10b) is relatively weak in the late winter, with most of the regions not reaching the level of significance. The exception appears in the subtropical western North Pacific and the southeastern coast region of North America, which may be related to the AO circulation anomaly, through positive air-sea feedback mechanism (Wu and Kinter, 2010; Xie and Philander, 1994).

6. Discussion and conclusions

Compared with the two-dimensional EP flux, the three-dimensional EP flux can be used to study the geographical characteristics of planetary wave activities and to investigate the regional effects. In addition to the sum of the wave activity flux of individual waves used for two-dimensional EP, the three-dimensional EP flux contains the interactions among different waves. The three-dimensional EP fluxes mainly show upward fluxes from the eastern part of the Eurasian continent in the early winter months, while in the mid-winter and late winter months, there are upward wave fluxes above Eurasia and downward wave fluxes above NANA. The decomposition of the 3D wave activity flux indicates that this pattern is due to wave-wave interaction, especially the action of wavenumber 2 to wavenumber 1. With the seasonal evolution in the boreal cold season, the pattern remains with slight change in different months.

In the early winter months, the interannual variation in the EP flux in the stratosphere is mainly featured by a strength change in the upward wave flux. However, in the mid and late winter months, it is mainly characterized by a dipole pattern, i.e., a wave flux oscillation between Eurasia and North America-North Atlantic. In early winter, the upward wave flux shows a leading relationship with the westerly jet strength in the

middle and upper stratosphere, with a stronger EP flux leading to a weaker polar vortex and weaker EP flux leading to a stronger polar jet. The EPz decomposition indicates that the effects of the early winter EP flux on mid-winter circumpolar westerly are mainly contributed by PW amplitude change.

In the mid-winter and late winter months, however, the strength of the stratospheric jet has a one-month leading relationship with the 3D EP flux dipole pattern in the lower stratosphere. When the jet is stronger, the dynamic coupling between the stratosphere and troposphere is enhanced, with a stronger upward flux above Eurasia and strong downward flux over North America and the North Atlantic region. Correspondingly, when the stratosphere westerly jet is weak or reversed to an easterly, the dynamic coupling between the stratosphere and troposphere is weakened in the following month, with a weaker upward EP flux from Eurasia and weaker downward EP flux above North America and the Atlantic. This dipole pattern is mainly contributed by the wave-wave interaction component of the EP flux, especially the action of PW2 on PW1. This dipole pattern of wave flux along the latitude circle is caused by the structure and amplitude change of both PW1 and PW2 in the stratosphere in January and February.

In the early winter months, the upward EP flux from the troposphere into the stratosphere is closely associated with the Scandinavian wave train pattern, which corresponds to a negative temperature anomaly in Siberia and Northeast Asia and a positive temperature anomaly in Eastern Europe and northern Europe. This is correlated with amplitude change of both planetary waves and synoptical waves, and with the SST anomaly over the central North Pacific. The SPV strength change in mid and late winter has a lagging effect on the wave flux between the stratosphere and troposphere. The first EOF mode of the 3D EP flux at the lower stratosphere is related to an AO-type circulation anomaly in the lower atmosphere, causing positive temperature anomalies in northern Europe, eastern United States and northeastern China and negative temperature anomalies in the Caspian Sea and northern North America.

Planetary wave activities provide a dynamic linkage between the stratosphere and

troposphere. The stratosphere circulation, especially the state of the SPV, is affected by the planetary waves from the troposphere. Conversely, stratospheric circulation can cause lagged regional circulation anomalies in the lower troposphere by modulating the amplitude and distribution of planetary and synoptic scale waves. The tropospheric impact of SSW events is communicated by a range of mechanisms including synoptic- and planetary scale wave (Domeisen *et al.*, 2020b; Hitchcock and Simpson, 2014; Smith and Scott, 2016; Song and Robinson, 2004). Notably, the circulation pattern caused by the 3D EP flux anomaly is very close to the AO-like anomaly at the lower levels. Therefore, it is necessary to distinguish the different effects from the stratosphere and lower troposphere, which is the key process in the study of the dynamic interaction between the stratosphere and troposphere.

Declarations

Funding

This research is supported by the Natural Science Foundation of China (Grant No. 4181101164, 41461144001 and 41861144016).

Conflict of interest

The authors declare that they have no conflict of interest.

Availability of data and material

The data is available from the authors upon request

Code availability

The code for diagnostics is available from the authors upon request

References

Andrews DG, McIntyre ME（1976) Planetary waves in horizontal and vertical shear: The generalized Eliassen-Palm relation and the mean zonal acceleration. Journal of the Atmospheric Sciences 33: 2031–2048.

Andrews DG, McIntyre ME（1978) Generalized Eliassen-Palm and Charney-Drazin theorems for waves on axisymmetric mean flows in compressible atmospheres. Journal of the Atmospheric Sciences 35: 175-185.

Anstey JA, Shepherd TG（2014) High-latitude influence of the quasi-biennial oscillation. Quarterly Journal of the Royal Meteorological Society 140(678): 1-21. doi: 10.1002/qj.2132

Anstey JA, Shepherd TG, Scinocca JF（2010) Influence of the Quasi-Biennial Oscillation on the Extratropical Winter Stratosphere in an Atmospheric General Circulation Model and in Reanalysis Data. Journal of the Atmospheric Sciences 67(5): 1402-1419. doi: 10.1175/2009jas3292.1

Ayarzagüena B, Palmeiro FM, Barriopedro D, Calvo N, Langematz U, Shibata K（2019) On the representation of major stratospheric warmings in reanalyses. Atmospheric Chemistry and Physics 19: 9469-9484.

Baldwin MP, Dunkerton TJ（2001) Stratospheric Harbingers of Anomalous Weather Regimes. Science 294(5542): 581-584. doi: 10.1126/science.1063315

Baldwin MP, Stephenson DB, Thompson DWJ, Dunkerton TJ, Charlton AJ, O'Neill A

（2003) Stratospheric Memory and Skill of Extended-Range Weather Forecasts. Science 301(5633): 636-640. doi: 10.1126/science.1087143

Baldwin MP, Birner T, Brasseur G, Burrows J, Butchart N, Garcia R, Geller M, Gray L, Hamilton K, Harnik N（2019) 100 years of progress in understanding the stratosphere and mesosphere. Meteorological Monographs 59: 27.21-27.62.

Baldwin MP, Gray LJ, Dunkerton TJ, Hamilton K, Haynes PH, Randel WJ, Molton JR, Alexander MJ, Hirota I, Horinouchi T, Jones DBA, Kinnersley JS, Marquardt C, Sato K, Takahashi M（2001) The quasi-biennial oscillation. Reviews of Geophysics 39(2): 179-229.

Barnes EA, Samarasinghe SM, Ebert-Uphoff I, Furtado JC（2019) Tropospheric and Stratospheric Causal Pathways Between the MJO and NAO. Journal of Geophysical Research-Atmospheres 124(16): 9356-9371. doi: 10.1029/2019jd031024

Beerli R, Grams CM（2019) Stratospheric modulation of the large-scale circulation in the Atlantic-European region and its implications for surface weather events. Quarterly Journal of the Royal Meteorological Society 145(725): 3732-3750. doi: 10.1002/qj.3653

Bueh C, Nakamura H（2007) Scandinavian pattern and its climatic impact. Quarterly Journal of the Royal Meteorological Society 133(629): 2117-2131. doi: 10.1002/qj.173

Butler AH, Polvani LM, Deser C（2014) Separating the stratospheric and tropospheric pathways of El Nino-Southern Oscillation teleconnections. Environmental Research Letters 9(2), 024014. doi: 10.1088/1748-9326/9/2/024014

Cagnazzo C, Manzini E（2009) Impact of the Stratosphere on the Winter Tropospheric Teleconnections between ENSO and the North Atlantic and European Region. Journal of Climate 22(5): 1223–1238. doi: 10.1175/2008jcli2549.1

Charney JG, Drazin PG（1961) Propagation of planetary-scale disturbances from the lower into the upper atmosphere. J Geophys Res 66: 83-109.

Chen W, Wei K（2009) Anomalous Propagation of the Quasi-stationary Planetary Waves in the Atmosphere and Its Roles in the Impact of the Stratosphere on the East Asian Winter Climate. Advances in Earth Science 24(3): 272-285. (in Chinese)

Chen W, Takahashi M, Graf HF（2003) Interannual variations of stationary planetary wave activity in the northern winter troposphere and stratosphere and their relations to NAM and SST. Journal of Geophysical Research 108(D24), 4797: 4797. doi: 10.1029/2003JD003834

Christiansen B（2001) Downward propagation of zonal mean zonal wind anomalies from the stratosphere to the troposphere: Model and reanalysis. Journal of Geophysical Research 106(D21): 27307-27322. doi: 10.1029/2000JD000214

Cohen J, Furtado JC, Jones J, Barlow M, Whittleston D, Entekhabi D（2014) Linking Siberian Snow Cover to Precursors of Stratospheric Variability. Journal of Climate 27(14): 5422-5432. doi: 10.1175/jcli-d-13-00779.1

De B, Wu Y（2019) Robustness of the stratospheric pathway in linking the Barents-Kara Sea sea ice variability to the mid-latitude circulation in CMIP5 models. Climate Dynamics 53(1-2): 193-207. doi: 10.1007/s00382-018-4576-6

Domeisen DI, Grams CM, Papritz L（2020a) The role of North Atlantic–European weather regimes in the surface impact of sudden stratospheric warming events. Weather and Climate Dynamics 1(2): 373-388.

Domeisen DIV, Garfinkel CI, Butler AH（2019) The Teleconnection of El Nino Southern Oscillation to the Stratosphere. Reviews of Geophysics 57(1): 5-47. doi: 10.1029/2018rg000596

Domeisen DIV, Butler AH, Charlton-Perez AJ, Ayarzaguena B, Baldwin MP, Dunn-Sigouin E, Furtado JC, Garfinkel CI, Hitchcock P, Karpechko AY, Kim H, Knight J, Lang AL, Lim E-P, Marshall A, Roff G, Schwartz C, Simpson IR, Son S-W, Taguchi M（2020b) The Role of the Stratosphere in Subseasonal to Seasonal Prediction: 2. Predictability Arising From Stratosphere-Troposphere Coupling. Journal of Geophysical Research-Atmospheres 125(2), e2019JD030923. doi: 10.1029/2019jd030923

Ebita A, Kobayashi S, Ota Y, Moriya M, Kumabe R, Onogi K, Harada Y, Yasui S, Miyaoka K, Takahashi K, Kamahori H, Kobayashi C, Endo H, Soma M, Oikawa Y, Ishimizu T（2011) The Japanese 55-year Reanalysis "JRA-55": An Interim Report. Sola 7: 149-152. doi: 10.2151/sola.2011-038

Edmon HJ, Jr., Hoskins BJ, McIntyre ME（1980) Eliassen-Palm cross sections for the troposphere. Journal of the Atmospheric Sciences 37(12): 2600–2616.

Eliassen A, Palm E（1961) On the Transfer of Energy in Stationary Mountain Waves. Geophys Publ 22: 1-23.

Ern M, Quang Thai T, Kaufmann M, Krisch I, Preusse P, Ungermann J, Zhu Y, Gille JC, Mlynczak MG, Russell JM, III, Schwartz MJ, Riese M（2016) Satellite observations of middle atmosphere gravity wave absolute momentum flux and of its vertical gradient during recent stratospheric warmings. Atmospheric Chemistry and Physics 16(15): 9983-10019. doi: 10.5194/acp-16-9983-2016

Fletcher CG, Cassou C（2015) The Dynamical Influence of Separate Teleconnections from the Pacific and Indian Oceans on the Northern Annular Mode. Journal of Climate 28(20): 7985-8002. doi: 10.1175/jcli-d-14-00839.1

Funke B, Ball W, Bender S, Gardini A, Harvey VL, Lambert A, López-Puertas M, Marsh DR, Meraner K, Nieder H（2017) HEPPA-II model–measurement

intercomparison project: EPP indirect effects during the dynamically perturbed NH winter 2008–2009. Atmospheric Chemistry and Physics 17(5): 3573-3604.

Hardiman SC, Dunstone NJ, Scaife AA, Smith DM, Knight JR, Davies P, Claus M, Greatbatch RJ（2020) Predictability of European winter 2019/20: Indian Ocean dipole impacts on the NAO. Atmospheric Science Letters, e1005. doi: 10.1002/asl.1005

Hell MC, Schneider T, Li C（2020) Atmospheric Circulation Response to Short-Term Arctic Warming in an Idealized Model. Journal of the Atmospheric Sciences 77(2): 531-549. doi: 10.1175/jas-d-19-0133.1

Hitchcock P, Simpson IR（2014) The Downward Influence of Stratospheric Sudden Warmings. Journal of the Atmospheric Sciences 71(10): 3856-3876. doi: 10.1175/jas-d-14-0012.1

Huang B, Thorne P, Banzon V, Boyer T, Chepurin G, Lawrimore J, Menne M, Smith T, Vose R, Zhang H（2017) NOAA Extended Reconstructed Sea Surface Temperature (ERSST). Information NNCfE, editor Version 5. doi: 10.7289/V5T72FNM

Hurwitz MM, Newman PA, Garfinkel CI（2012) On the influence of North Pacific sea surface temperature on the Arctic winter climate. Journal of Geophysical Research-Atmospheres 117, D19110. doi: 10.1029/2012jd017819

Hurwitz MM, Calvo N, Garfinkel CI, Butler AH, Ineson S, Cagnazzo C, Manzini E, Pena-Ortiz C（2014) Extra-tropical atmospheric response to ENSO in the CMIP5 models. Climate Dynamics 43(12): 3367–3376. doi: 10.1007/s00382-014-2110-z

Ineson S, Scaife AA（2009) The role of the stratosphere in the European climate response to El Nino. Nature Geoscience 2(1): 32-36. doi: 10.1038/ngeo381

Jadin EA（2011) Stratospheric “wave hole” and interannual variations of the stratospheric circulation in late winter. Natural Science 3(04): 259-267.

Jadin EA, Wei K, Zyulyaeva YA, Chen W, Wang L（2010) Stratospheric wave activity and the Pacific Decadal Oscillation. Journal of Atmospheric and Solar-Terrestrial Physics 72(16): 1163-1170. doi: 10.1016/j.jastp.2010.07.009

Karoly DJ（1982) Eliassen-Palm cross sections for the northern and southern hemispheres. Journal of the Atmospheric Sciences 39(1): 178-182. doi: 10.1175/1520-0469(1982)039<0178:epcsft>2.0.co;2

Karoly DJ, Plumb RA, Ting MF（1989) Examples of the Horizontal Propagation of Quasi-stationary Waves. Journal of the Atmospheric Sciences 46(18): 2802-2811. doi: 10.1175/1520-0469(1989)046<2802:eothpo>2.0.co;2

Kiehl JT, Solomon S（1986) On the Radiative Balance of the Stratosphere. Journal of the Atmospheric Sciences 43(14): 1525-1534. doi: 10.1175/1520-

0469(1986)043<1525:OTRBOT>2.0.CO;2

Kim H-J, Son S-W（2020) Recent Eurasian winter temperature change and its association with Arctic sea-ice loss. Polar Research 39, 3363. doi: 10.33265/polar.v39.3363

Kim J, Kim K-Y（2020) Characteristics of stratospheric polar vortex fluctuations associated with sea ice variability in the Arctic winter. Climate Dynamics 54(7-8): 3599-3611. doi: 10.1007/s00382-020-05191-9

Kinoshita T, Sato K（2013) A Formulation of Unified Three-Dimensional Wave Activity Flux of Inertia-Gravity Waves and Rossby Waves. Journal of the Atmospheric Sciences 70(6): 1603-1615. doi: 10.1175/jas-d-12-0138.1

Kinoshita T, Tomikawa Y, Sato K（2010) On the Three-Dimensional Residual Mean Circulation and Wave Activity Flux of the Primitive Equations. Journal of the Meteorological Society of Japan 88(3): 373-394. doi: 10.2151/jmsj.2010-307

Kodera K（2006) The role of dynamics in solar forcing. Space Science Reviews 125(1-4): 319-330. doi: 10.1007/s11214-006-9066-1

Kodera K, Kuroda Y（2002) Dynamical response to the solar cycle. Journal of Geophysical Research 107(D24), D4749. doi: 4710.1029/2002JD002224

Kodera K, Mukougawa H, Itoh S（2008) Tropospheric impact of reflected planetary waves from the stratosphere. Geophysical Research Letters 35(16). doi: 10.1029/2008gl034575

Kodera K, Mukougawa H, Fujii A（2013) Influence of the vertical and zonal propagation of stratospheric planetary waves on tropospheric blockings. Journal of Geophysical Research-Atmospheres 118(15): 8333-8345. doi: 10.1002/jgrd.50650

Kuroda Y, Kodera K（1999) Role of planetary waves in the stratosphere-troposphere coupled variability in the Northern Hemisphere winter. Geophys Res Lett 26: 2375-2378.

Liu Y, Wang L, Zhou W, Chen W（2014) Three Eurasian teleconnection patterns: spatial structures, temporal variability, and associated winter climate anomalies. Climate Dynamics 42: 2817-2839. doi: 10.1007/s00382-014-2163-z

Overland JE, Wang M（2019) Impact of the winter polar vortex on greater North America. International Journal of Climatology 39(15): 5815-5821. doi: 10.1002/joc.6174

Pedatella N, Chau J, Schmidt H, Goncharenko L, Stolle C, Hocke K, Harvey V, Funke B, Siddiqui T（2018) How Sudden stratospheric warmings affect the whole atmosphere. EOS 99(6). doi: 10.1029/2018EO092441

Peters D, Vargin P（2015) Impact of extratropical Rossby wave trains on planetary wave activity in the polar southern lower stratosphere in September 2002. Tellus A 67.

Peters D, Vargin P, Körnich H（2007) A study of the zonally asymmetric tropospheric forcing of the austral vortex splitting during September 2002. Tellus A: Dynamic Meteorology and Oceanography 59(3): 384-394.

Peters D, Vargin P, Gabriel A, Tsvetkova N, Yushkov V（2010) Tropospheric forcing of the boreal polar vortex splitting in January 2003. Annales Geophysicae 28(11): 2133-2148. doi: 10.5194/angeo-28-2133-2010

Plumb RA（1985) On the Three-Dimensional Propagation of Stationary Waves. Journal of Atmospheric Sciences 42(3): 217-229.

Randel WJ, Williamson DL（1990) A Comparison of the Climate Simulated by the NCAR Community Climate Model (CCM1-R15) with ECMWF Analyses. Journal of Climate 3(6): 608-633. doi: 10.1175/1520-0442(1990)003<0608:Acotcs>2.0.Co;2

Ren R-C（2012) Seasonality of the Lagged Relationship between ENSO and the Northern Hemispheric Polar Vortex Variability. Atmospheric and Oceanic Science Letters 5(2): 113-118.

Ren RC, Cai M, Xiang CY, Wu GX（2012) Observational evidence of the delayed response of stratospheric polar vortex variability to ENSO SST anomalies. Climate Dynamics 38(7-8): 1345-1358. doi: 10.1007/s00382-011-1137-7

Smith KL, Scott RK（2016) The role of planetary waves in the tropospheric jet response to stratospheric cooling. Geophysical Research Letters 43(6): 2904-2911. doi: 10.1002/2016gl067849

Song L, Wu R（2020) Modulation of the Westerly and Easterly Quasi-Biennial Oscillation Phases on the Connection between the Madden-Julian Oscillation and the Arctic Oscillation. Atmosphere 11(2), 175. doi: 10.3390/atmos11020175

Song Y, Robinson WA（2004) Dynamical Mechanisms for Stratospheric Influences on the Troposphere. Journal of Atmospheric Sciences 61(14): 1711-1725. doi: DOI: 10.1175/1520-0469(2004)061<1711:DMFSIO>2.0.CO;2

Takaya K, Nakamura H（1997) A formulation of a wave-activity flux for stationary Rossby waves on a zonally varying basic flow. Geophysical Research Letters 24(23): 2985-2988. doi: 10.1029/97gl03094

Takaya K, Nakamura H（2001) A Formulation of a Phase-Independent Wave-Activity Flux for Stationary and Migratory Quasigeostrophic Eddies on a Zonally Varying Basic Flow. Journal of Atmospheric Sciences 58(6): 608-627.

Teng H, Branstator G, Wang H, Meehl GA, Washington WM（2013) Probability of US

heat waves affected by a subseasonal planetary wave pattern. Nature Geoscience 6(12): 1056-1061. doi: 10.1038/ngeo1988

Thompson DWJ, Wallace JM（2000) Annular Modes in the Extratropical Circulation. Part I: Month-to-Month Variability. Journal of Climate 13(5): 1000–1016.

Thompson DWJ, Baldwin MP, Wallace JM（2002) Stratospheric Connection to Northern Hemisphere Wintertime Weather: Implications for Prediction. Journal of Climate 15(12): 1421-1428.

Toniazzo T, Scaife AA（2006) The influence of ENSO on winter North Atlantic climate. Geophysical Research Letters 33(24), L24704. doi: 10.1029/2006gl027881

Weare BC（2010) Tropospheric-stratospheric wave propagation during El Nino-Southern Oscillation. Journal of Geophysical Research-Atmospheres 115, D18122. doi: 10.1029/2009jd013647

Wei K, Chen W（2012) Northern Hemisphere Stratospheric Polar Vortex Extremes in February under the Control of Downward Wave Flux in the Lower Stratosphere. Atmospheric and Oceanic Science Letters 5(3): 183-188.

Wei K, Chen W, Huang RH（2007) Association of tropical Pacific sea surface temperatures with the stratospheric Holton-Tan Oscillation in the Northern Hemisphere winter. Geophysical Research Letters 34(16), L16814. doi: 10.1029/2007gl030478|issn 0094-8276

Wu R, Kinter JL, III（2010) Atmosphere-ocean relationship in the midlatitude North Pacific: Seasonal dependence and east-west contrast. Journal of Geophysical Research-Atmospheres 115, D06101. doi: 10.1029/2009jd012579

Xie SP, Philander SGH（1994) A coupled ocean-atmosphere model of relevance to the ITCZ in the Eastern Pacific. Tellus Series a-Dynamic Meteorology and Oceanography 46(4): 340-350. doi: 10.1034/j.1600-0870.1994.t01-1-00001.x

Yang S, Gutowski WJ（1994) GCM Simulations of the Three-Dimensional Propagation of Stationary Waves. Journal of Climate 7: 414-433.

Zhang P, Wu Y, Smith KL（2018) Prolonged effect of the stratospheric pathway in linking Barents-Kara Sea sea ice variability to the midlatitude circulation in a simplified model. Climate Dynamics 50(1-2): 527-539. doi: 10.1007/s00382-017-3624-y

Zhou P, Suo L, Yuan J, Tan B（2012) The East Pacific Wavetrain: Its variability and impact on the atmospheric circulation in the boreal winter. Advances in Atmospheric Sciences 29(3): 471-483. doi: 10.1007/s00376-011-0216-3

Zhou X, Chen Q, Wang Z, Xu M, Zhao S, Cheng Z, Feng F（2020) Longer Duration of the Weak Stratospheric Vortex During Extreme El Nino Events Linked to Spring

Eurasian Coldness. Journal of Geophysical Research-Atmospheres 125(16), e2019JD032331. doi: 10.1029/2019jd032331

Zyulyaeva YA, Jadin EA（2009) Analysis of three-dimensional Eliassen-Palm fluxes in the lower stratosphere. Russian Meteorology and Hydrology 8: 5-14. (http://ao.atmos.colostate.edu).

Tables

Table 1. Correlation coefficients of the strength of the stratospheric polar jet (zonal-mean zonal wind at 65ºN, 30 hPa) with the first EOF mode for the 30 hPa 3D EP flux vertical component.

PC1 of EPz	Jet strength				
	Nov	Dec	Jan	Feb	Mar
Nov	**−0. 584****	**−0. 446****	−0. 208	0. 070	0. 310*
Dec	−0. 268	**−0. 486****	−0. 484**	−0. 119	−0. 001
Jan	0. 169	0. 162	0. 156	0. 155	0. 182
Feb	0. 033	0. 091	0. 305*	0. 208	0. 026
Mar	0. 161	0. 296*	0. 080	0. 359*	−0. 082

Figure Captions:

Figure 1 The EP flux climatology at 30 hPa. Top panels: October and November; mid panels: December and January; bottom panels: February and March. The contours are the vertical component of the EP flux (unit: $m^2 s^{-2}$) with an interval of 0.1 $m^2 s^{-2}$, and the vectors are the horizontal component. The scales for the horizontal fluxes are 2 $m^2 s^{-2}$, as shown in the insets.

Figure 2 The EP flux climatology at 65 °N for the longitude-height section. Top panels: (a) October and (b) November; mid panels: (c) December and (d) January; bottom panels: (e) February and (f) March. The contours are the vertical component of the EP flux (unit: $m^2 s^{-2}$) with an interval of 0.1 $m^2 s^{-2}$, and the vectors are the zonal and vertical components. The scales for the horizontal fluxes are 2 $m^2 s^{-2}$, as shown in the insets.

Figure 3 (a) The wavenumber 1 component of the geopotential height at 65°N, (b) the wavenumber 2 component of the geopotential height at 65°N, and (c) the sum of wavenumber 1 and 2 of the geopotential height at 65°N.

Figure 4 The winter (DJF) EP flux climatology at 65 °N for the longitude-height section: (a) total wave flux, (b) the sum of flux caused by the individual waves, (c) the total wave flux caused by the wave-wave interaction, (d) the flux caused by wave 2 acting on wave 1 (EP (2, 1)), (e) wave 3 acting on wave 1 (EP (3, 1)), (f) wave 1 acting on wave 2 (EP (1, 2)), (g) wave 3 acting on wave 2 (EP(3, 2)), (h) wave 1 acting on wave 3 (EP (1, 3)), and (i) wave 2 acting on wave 3 (EP(2, 3)). The contours are the vertical component of the EP flux (unit: $m^2 s^{-2}$) with an interval of 0.002 $m^2 s^{-2}$, and the vectors are the zonal and vertical components. The scales for the horizontal fluxes are 2 $m^2 s^{-2}$, as shown in the insets. The vertical component of the vectors is scaled by the inverse of the air density.

Figure 5 The first EOF of the EPz at 30 hPa expressed as regressions with their corresponding principal component (PC). Top panels: October and November; mid

panels: December and January; bottom panels: February and March. Their contributions to the total variance are shown in the upper-right. The contours are the vertical component of the EP flux (unit: $m^2 s^{-2}$) with an interval of 0.002 $m^2 s^{-2}$, and the vectors are the horizontal component. The scales for the horizontal fluxes are 2 $m^2 s^{-2}$, as shown in the insets.

Figure 6 Hovmueller plot of the regression coefficient (contours) between (a) EPz at 30 hPa 65°N, (b) the EPz sum of wave activities from each wavenumber, (c) EPz from the interaction between waves, and (d) EPz from the action of wavenumber 2 on wavenumber 1 from October to April and the SPV index (zonal mean zonal wind at 65°N, 30 hPa) in January. Shadings indicate the region above the 95% statistically significant level.

Figure 7 The regression (shading) of the wave component of geopotential in December (upper panels), January (middle panels), and February (bottom panels) on the SPV index (zonal mean zonal wind at 65°N, 30 hPa) in January. Left: wavenumber 1. Right: wavenumber 2. Contours indicate the climatology of wave component in each month, and stippling shows the significant region above the 95% confidence level.

Figure 8 Longitude-height cross section of zonal wind (shading) and EP flux at 65°N composited according to the PC 1 of EPz at 30 hPa. The upper (a, b, c) panels are for the early winter of ND, and the bottom (d, e, f) panels are for the mid and late winter of JFM. (a) and (d) are composites of the positive PC1 phase, (b) and (e) are composites of the negative PC1 phase, and (c) and (f) are composite difference of the positive and negative phases, respectively.

Figure 9 Regression of temperature (shadings, unit: °C), geopotential height (contours) and horizontal wind field anomalies at 850 hPa on the leading principal component of EPz EOF mode of early winter (left panels, November and December) and mid and late winter (right panels, January, February and March). (a) and (b) are for the total wave components of geopotential height (contours) and horizontal wind field, (c) and (d) for the sum of wavenumber 1, 2 and 3, and (e) and (f) for the sum of

wavenumber greater than 3.

Figure 10 Regression of sea surface temperature (shadings, unit: °C) on the leading principal component of EPz EOF for (a) early winter, and (b) late winter. stippling shows the significant region above the 95% confidence level.

Figures

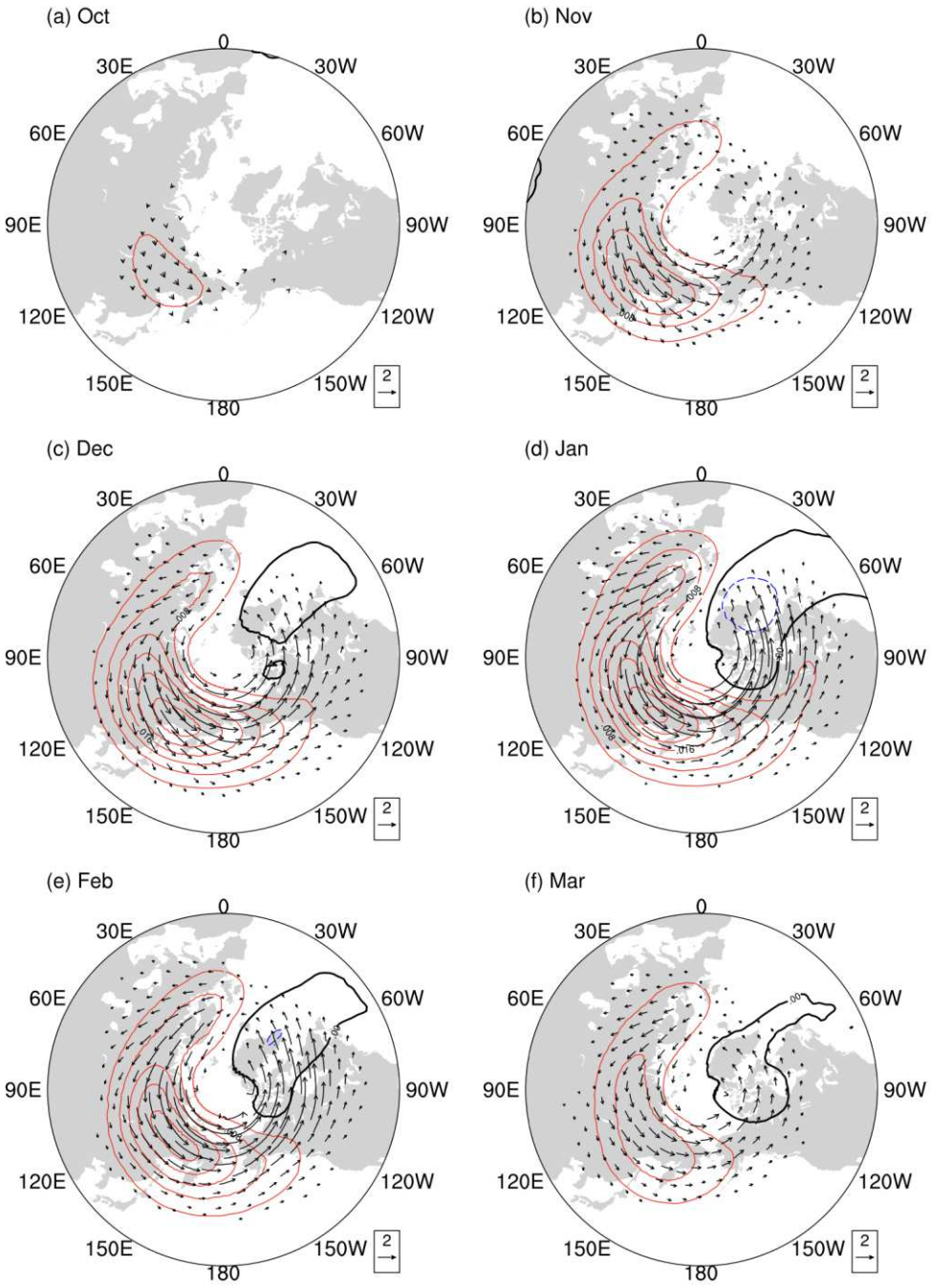

Figure 1 The EP flux climatology at 30 hPa. Top panels: October and November; mid panels: December and January; bottom panels: February and March. The contours are the vertical component of the EP flux (unit: $m^2\,s^{-2}$) with an interval of 0.1 $m^2\,s^{-2}$, and the vectors are the horizontal component. The scales for the horizontal fluxes are 2 $m^2\,s^{-2}$, as shown in the insets.

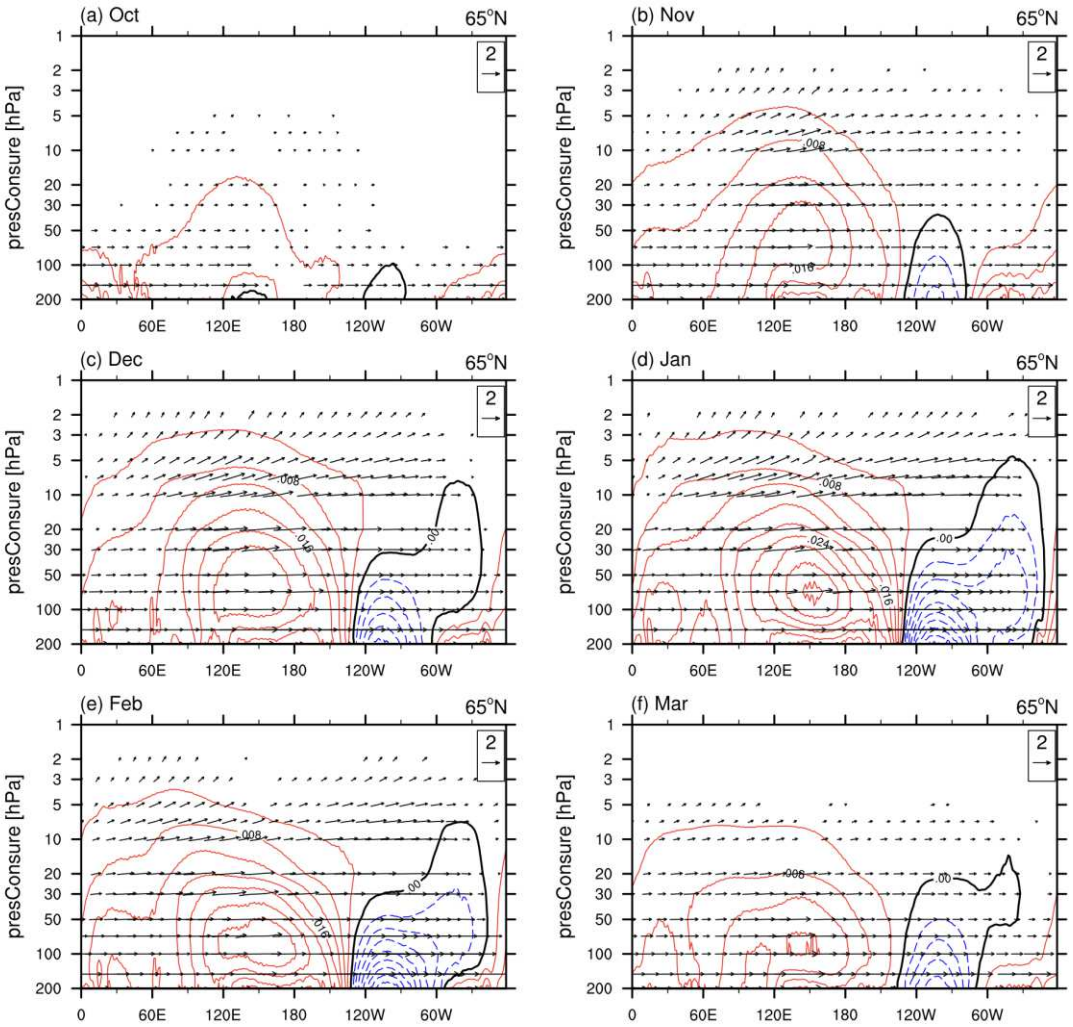

Figure 2 The EP flux climatology at 65 °N for the longitude-height section. Top panels: (a) October and (b) November; mid panels: (c) December and (d) January; bottom panels: (e) February and (f) March. The contours are the vertical component of the EP flux (unit: $m^2 s^{-2}$) with an interval of 0.1 $m^2 s^{-2}$, and the vectors are the zonal and vertical components. The scales for the horizontal fluxes are 2 $m^2 s^{-2}$, as shown in the insets.

□

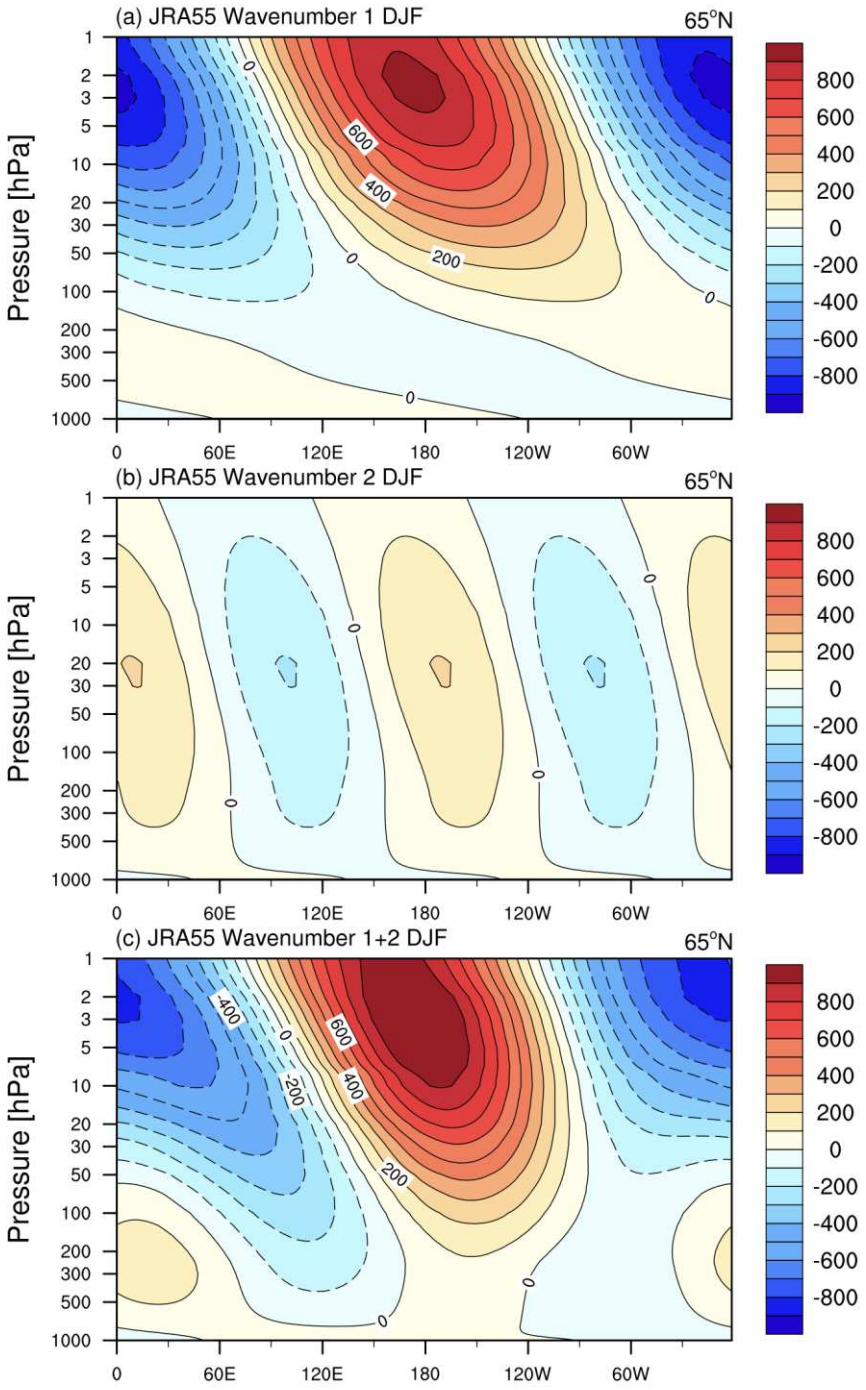

Figure 3 (a) The wavenumber 1 component of the geopotential height at 65°N, (b) the wavenumber 2 component of the geopotential height at 65°N, and (c) the sum of wavenumber 1 and 2 of the geopotential height at 65°N.

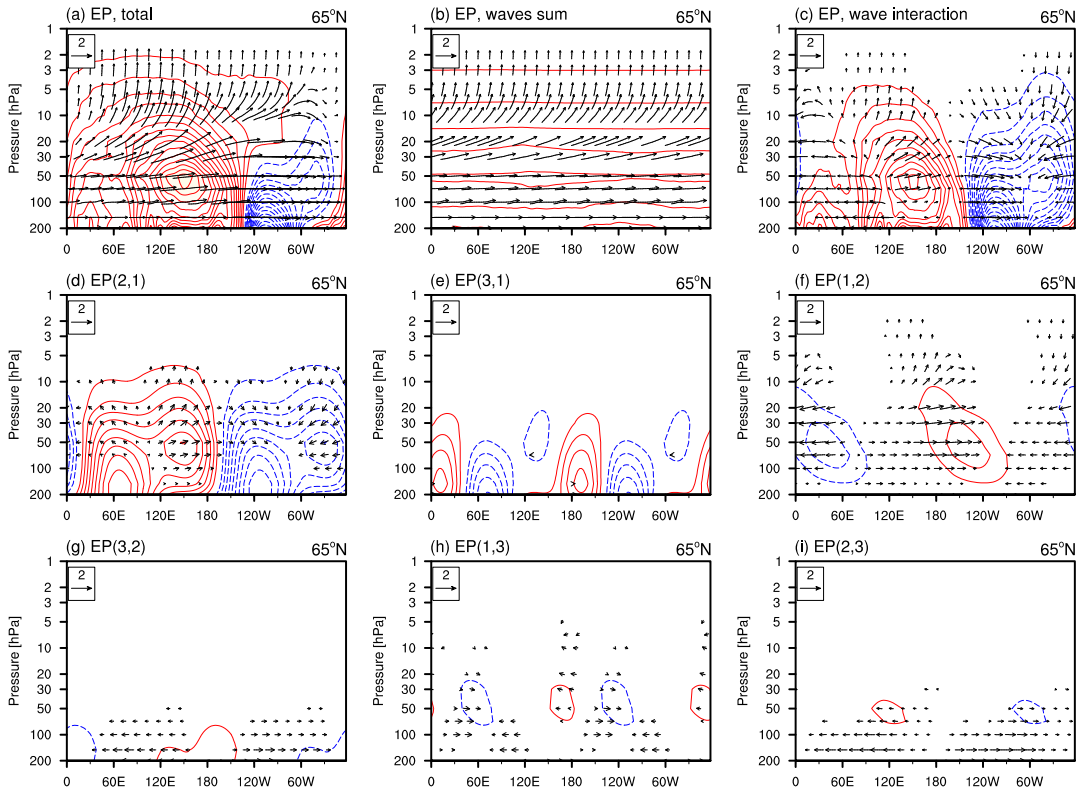

Figure 4 The winter (DJF) EP flux climatology at 65 °N for the longitude-height section: (a) total wave flux, (b) the sum of flux caused by the individual waves, (c) the total wave flux caused by the wave-wave interaction, (d) the flux caused by wave 2 acting on wave 1 (EP (2, 1)), (e) wave 3 acting on wave 1 (EP (3, 1)), (f) wave 1 acting on wave 2 (EP (1, 2)), (g) wave 3 acting on wave 2 (EP(3, 2)), (h) wave 1 acting on wave 3 (EP (1, 3)), and (i) wave 2 acting on wave 3 (EP(2, 3)). The contours are the vertical component of the EP flux (unit: $m^2\,s^{-2}$) with an interval of 0.002 $m^2\,s^{-2}$, and the vectors are the zonal and vertical components. The scales for the horizontal fluxes are 2 $m^2\,s^{-2}$, as shown in the insets. The vertical component of the vectors is scaled by the inverse of the air density.

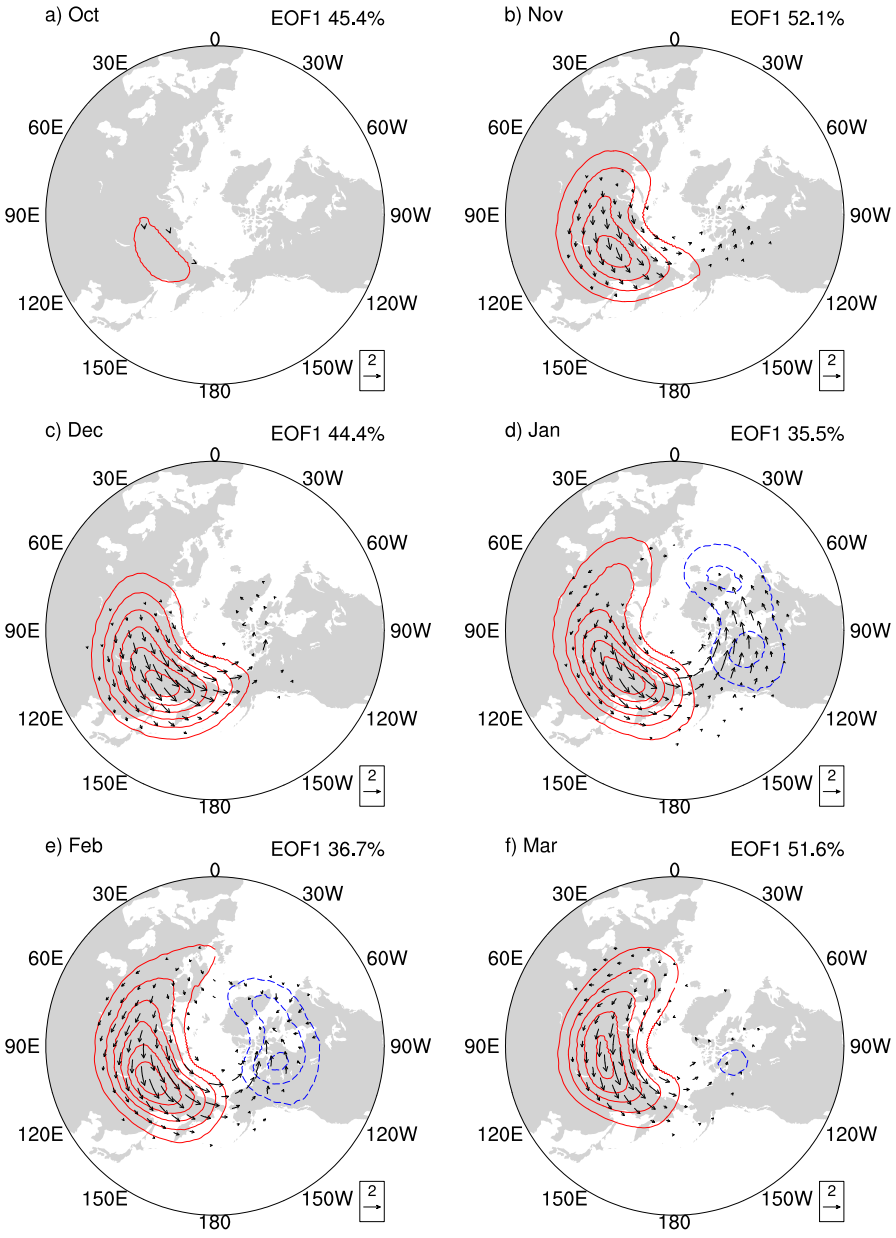

Figure 5 The first EOF of the EPz at 30 hPa expressed as regressions with their corresponding principal component (PC). Top panels: October and November; mid panels: December and January; bottom panels: February and March. Their contributions to the total variance are shown in the upper-right. The contours are the vertical component of the EP flux (unit: $m^2\,s^{-2}$) with an interval of 0.002 $m^2\,s^{-2}$, and the vectors are the horizontal component. The scales for the horizontal fluxes are 2 $m^2\,s^{-2}$, as shown in the insets.

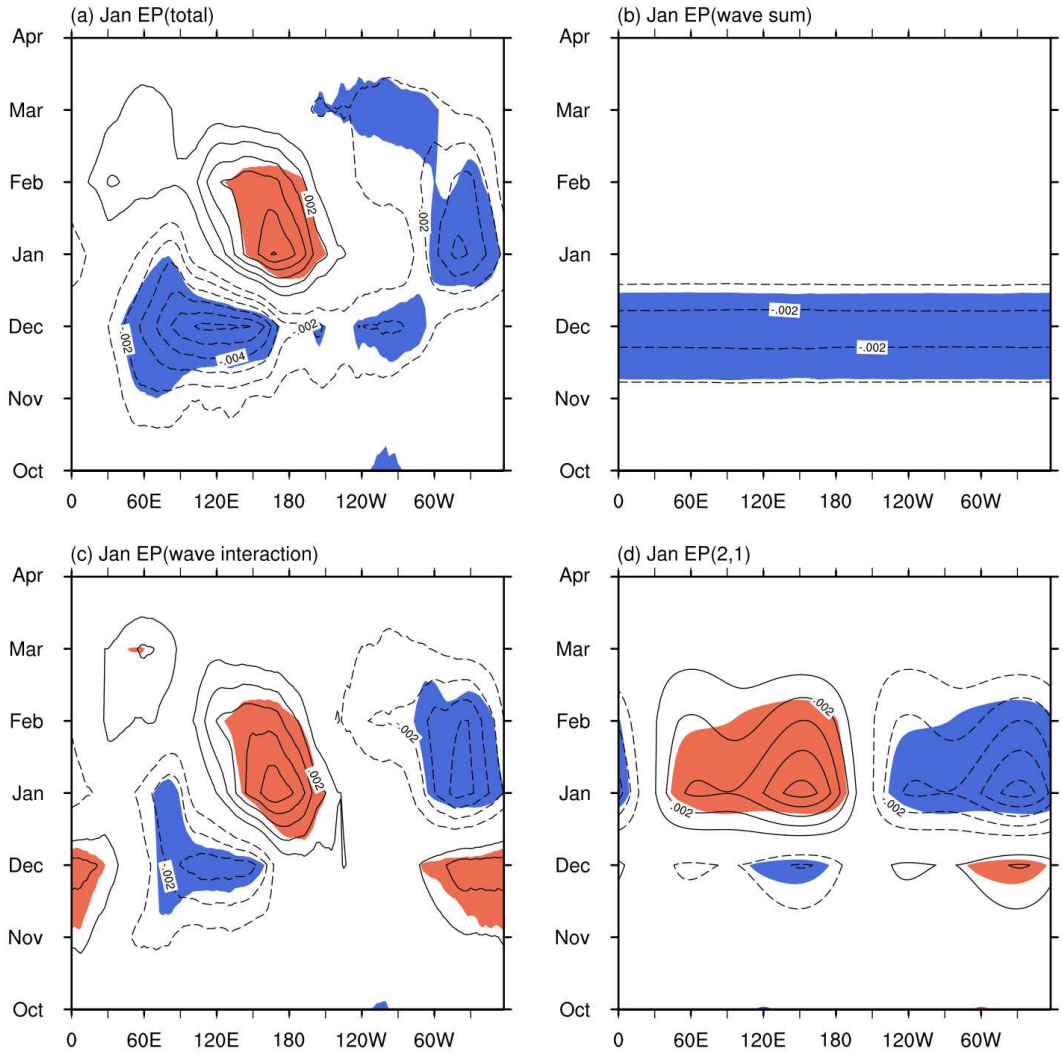

Figure 6 Hovmueller plot of the regression coefficient (contours) between (a) EPz at 30 hPa 65°N, (b) the EPz sum of wave activities from each wavenumber, (c) EPz from the interaction between waves, and (d) EPz from the action of wavenumber 2 on wavenumber 1 from October to April and the SPV index (zonal mean zonal wind at 65°N, 30 hPa) in January. Shadings indicate the region above the 95% statistically significant level.

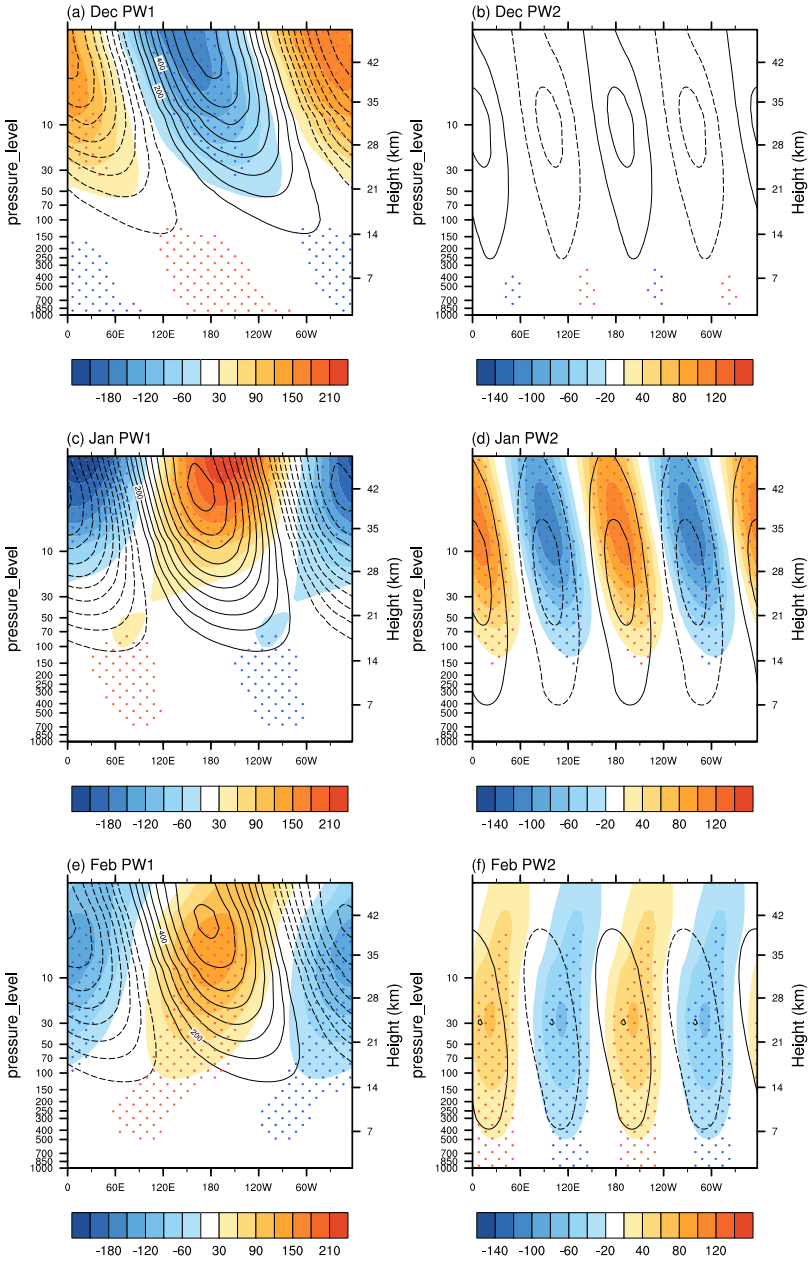

Figure 7 The regression (shading) of the wave component of geopotential in December (upper panels), January (middle panels), and February (bottom panels) on the SPV index (zonal mean zonal wind at 65°N, 30 hPa) in January. Left: wavenumber 1. Right: wavenumber 2. Contours indicate the climatology of wave component in each month, and stippling shows the significant region above the 95% confidence level.

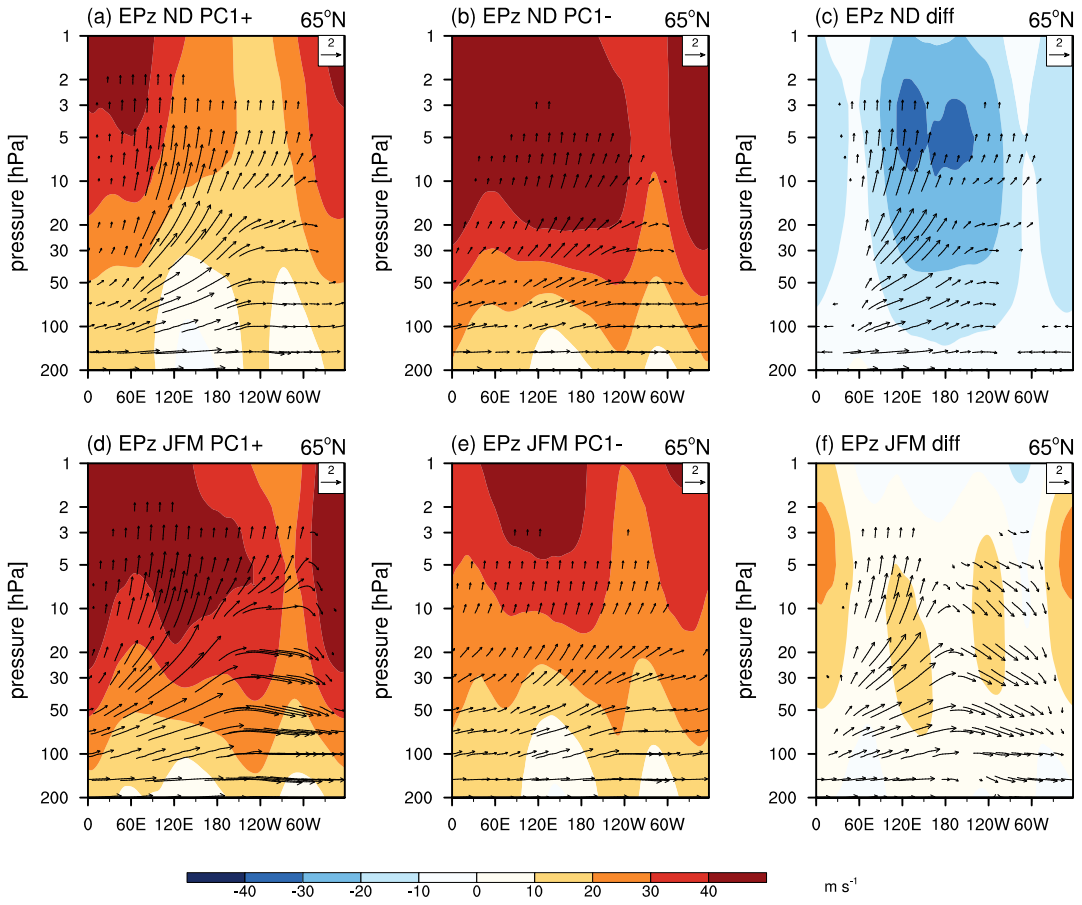

Figure 8 Longitude-height cross section of zonal wind (shading) and EP flux at 65°N composited according to the PC 1 of EPz at 30 hPa. The upper (a, b, c) panels are for the early winter of ND, and the bottom (d, e, f) panels are for the mid and late winter of JFM. (a) and (d) are composites of the positive PC1 phase, (b) and (e) are composites of the negative PC1 phase, and (c) and (f) are composite difference of the positive and negative phases, respectively.

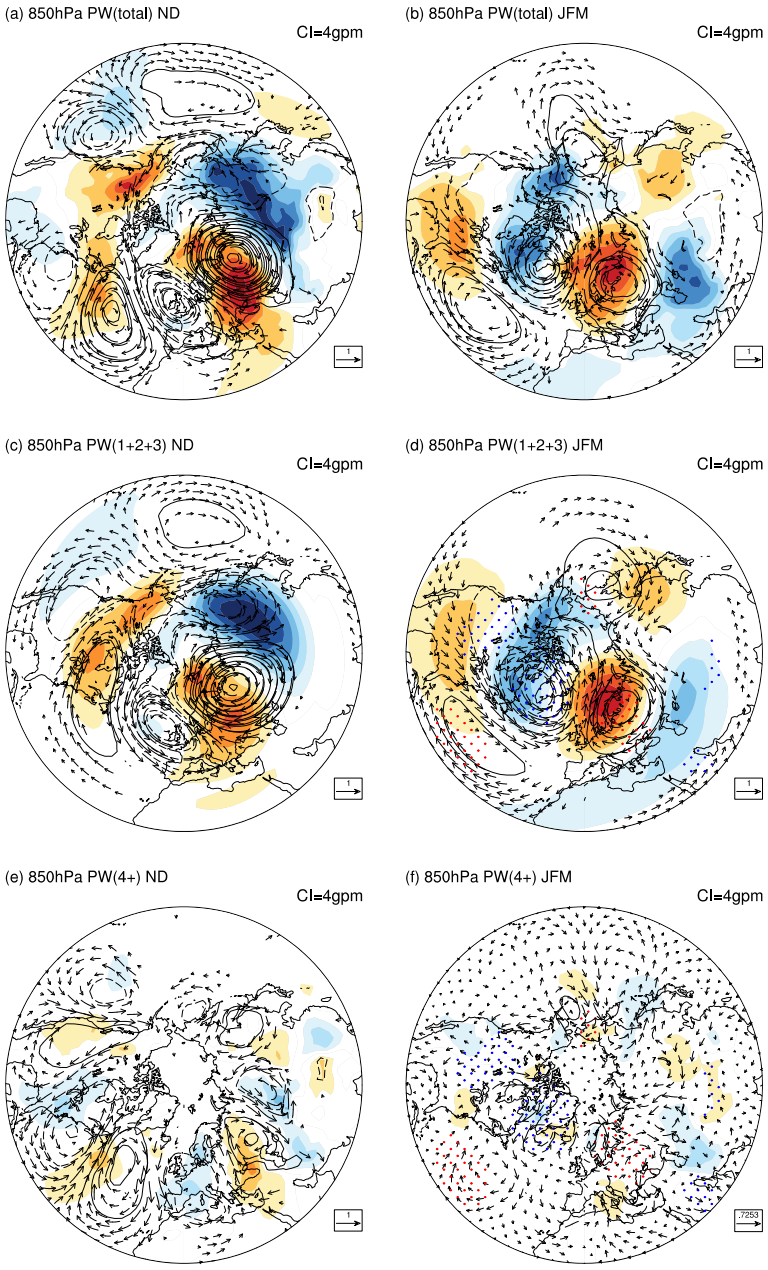

Figure 9 Regression of temperature (shadings, unit: °C), geopotential height (contours) and horizontal wind field anomalies at 850 hPa on the leading principal component of EPz EOF mode of early winter (left panels, November and December) and mid and late winter (right panels, January, February and March). (a) and (b) are for the total wave components of geopotential height (contours) and horizontal wind field, (c) and (d) for the sum of wavenumber 1, 2 and 3, and (e) and (f) for the sum of wavenumber greater than 3.

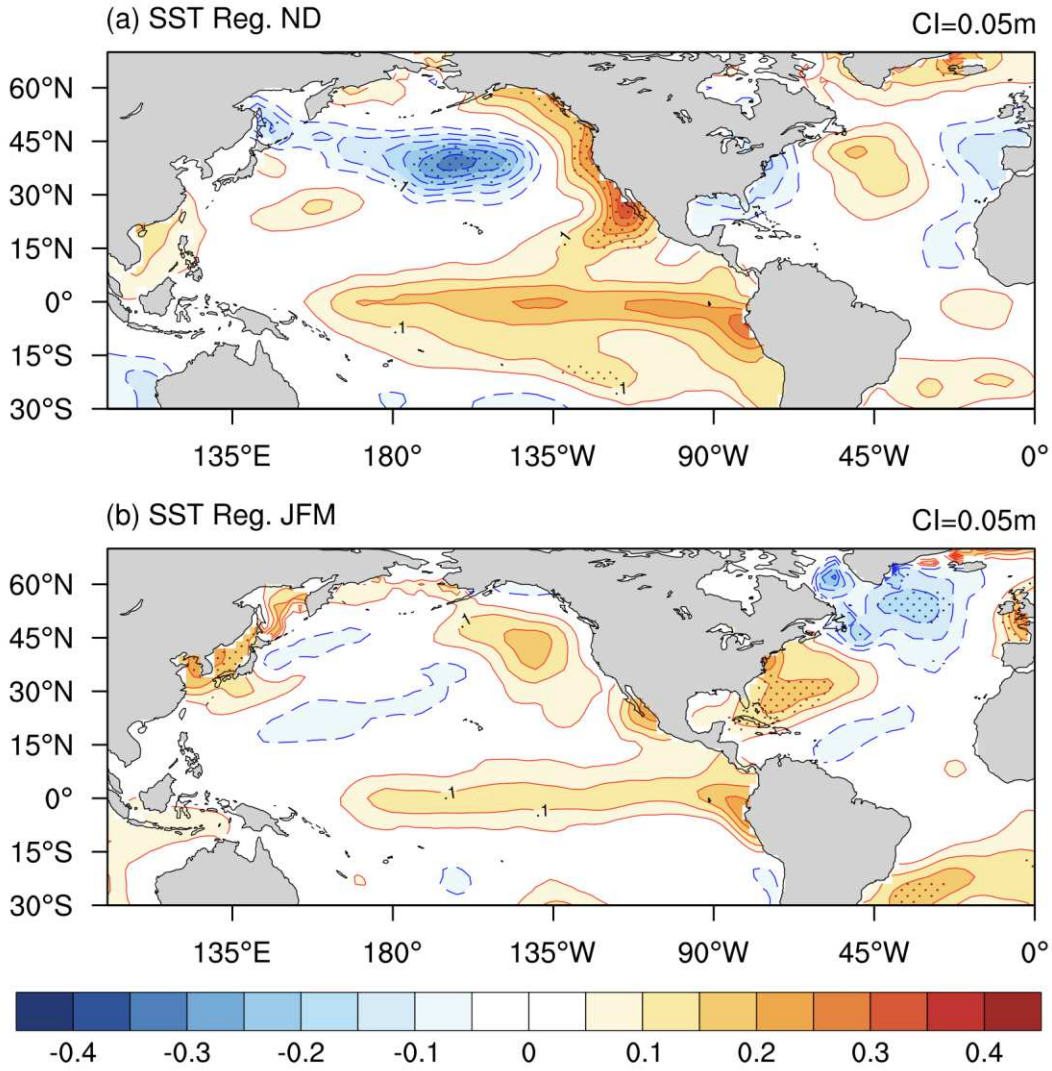

Figure 10 Regression of sea surface temperature (shadings, unit: °C) on the leading principal component of EPz EOF for (a) early winter, and (b) late winter. stippling shows the significant region above the 95% confidence level.

Figures

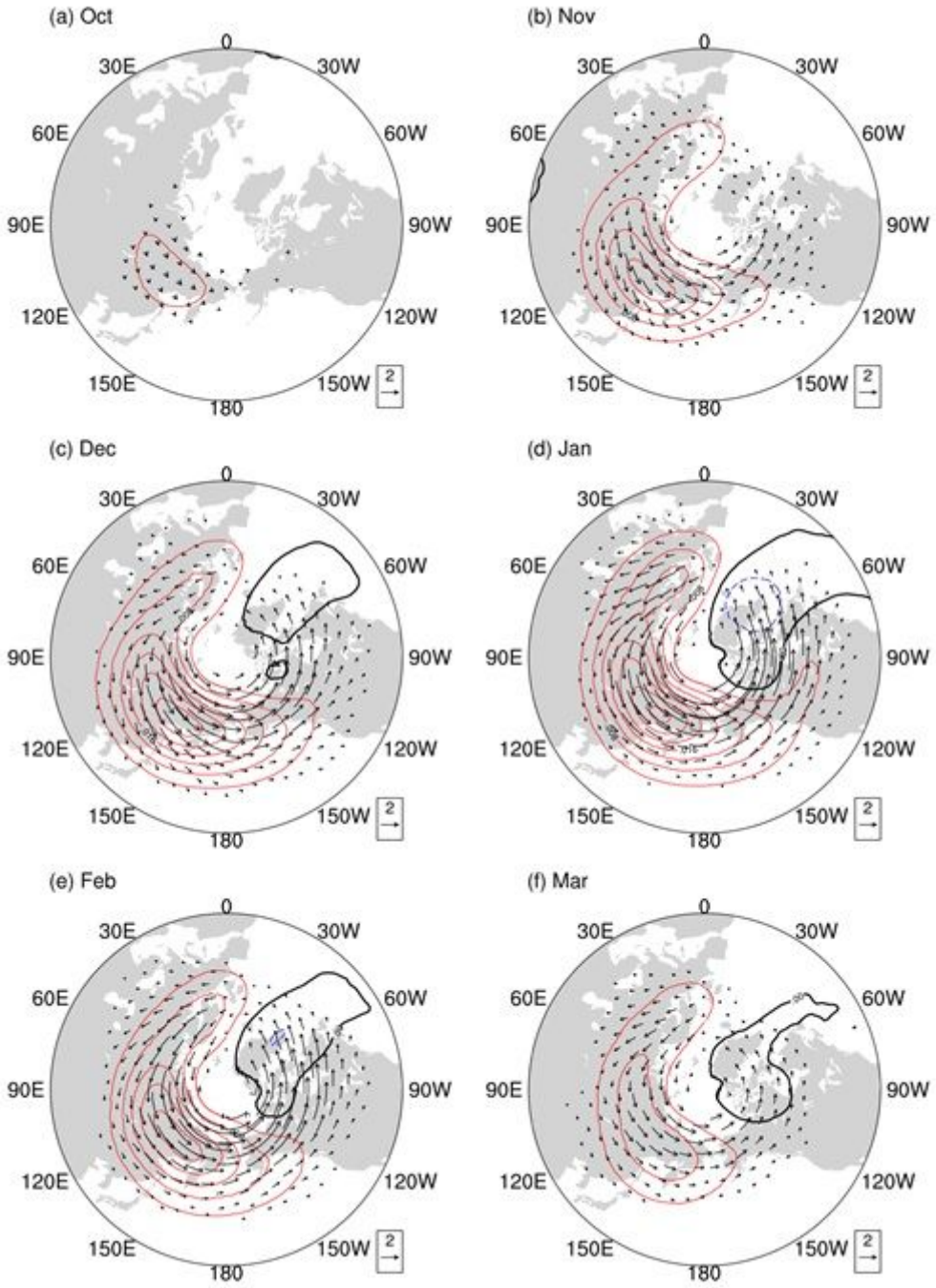

Figure 1

The EP flux climatology at 30 hPa. Top panels: October and November; mid panels: December and January; bottom panels: February and March. The contours are the vertical component of the EP flux (unit: m2 s-2) with an interval of 0.1 m2 s-2, and the vectors are the horizontal component. The scales for the horizontal fluxes are 2 m2 s-2, as shown in the insets. Note: The designations employed and the presentation of the material on this map do not imply the expression of any opinion whatsoever on the part of Research Square concerning the legal status of any country, territory, city or area or of its

authorities, or concerning the delimitation of its frontiers or boundaries. This map has been provided by the authors.

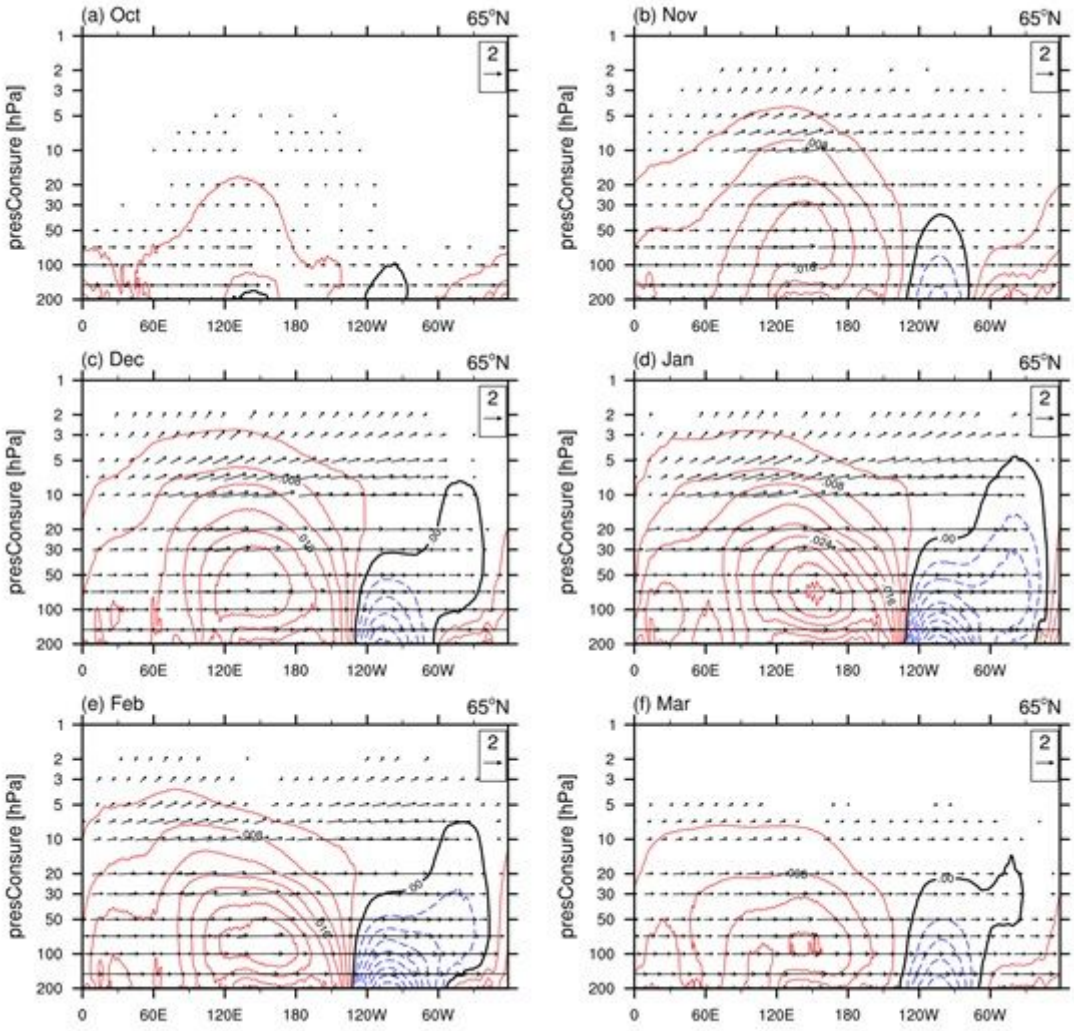

Figure 2

The EP flux climatology at 65 °N for the longitude-height section. Top panels: (a) October and (b) November; mid panels: (c) December and (d) January; bottom panels: (e) February and (f) March. The contours are the vertical component of the EP flux (unit: m2 s-2) with an interval of 0.1 m2 s-2, and the vectors are the zonal and vertical components. The scales for the horizontal fluxes are 2 m2 s-2, as shown in the insets.

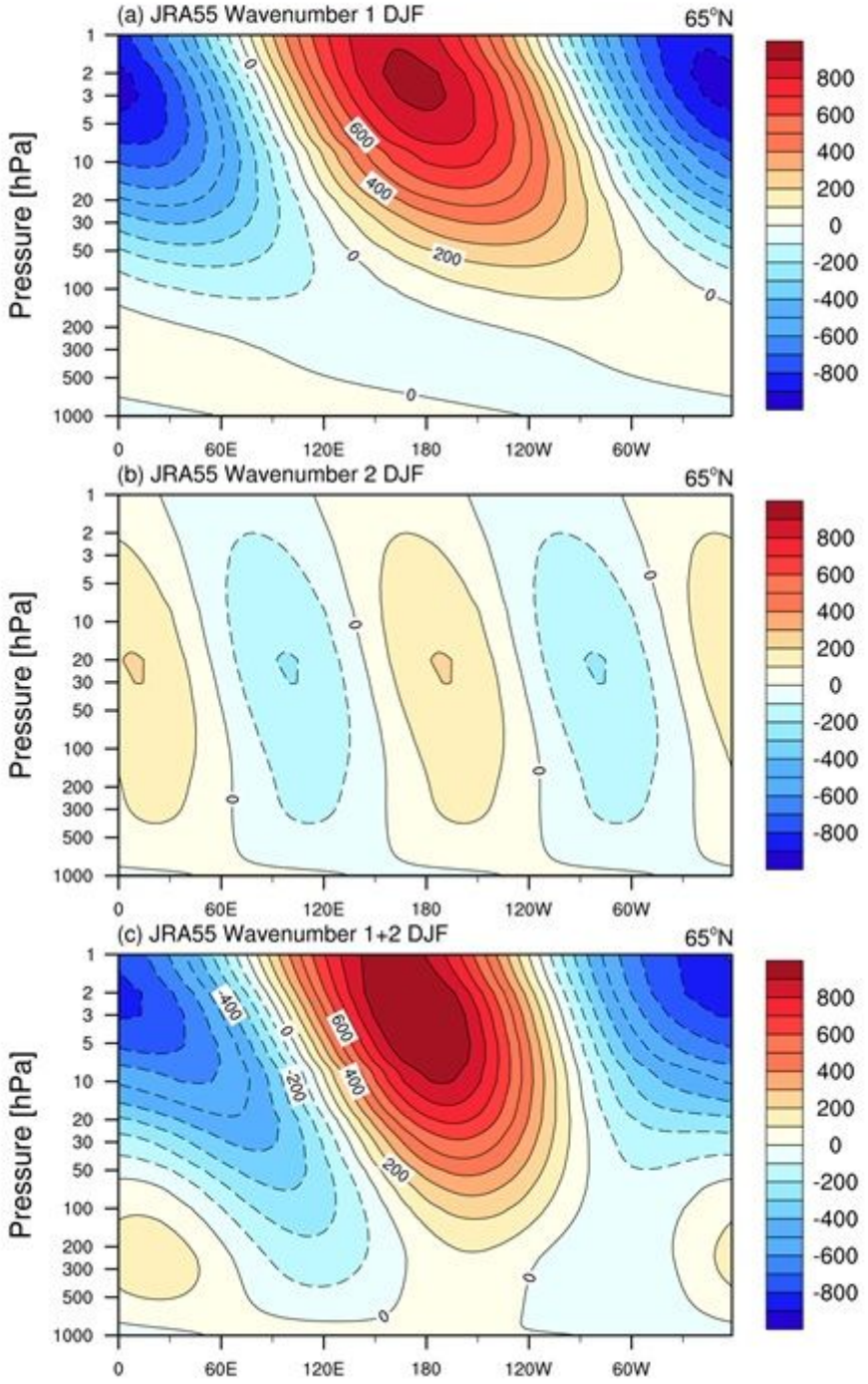

Figure 3

(a) The wavenumber 1 component of the geopotential height at 65°N, (b) the wavenumber 2 component of the geopotential height at 65°N, and (c) the sum of wavenumber 1 and 2 of the geopotential height at 65°N.

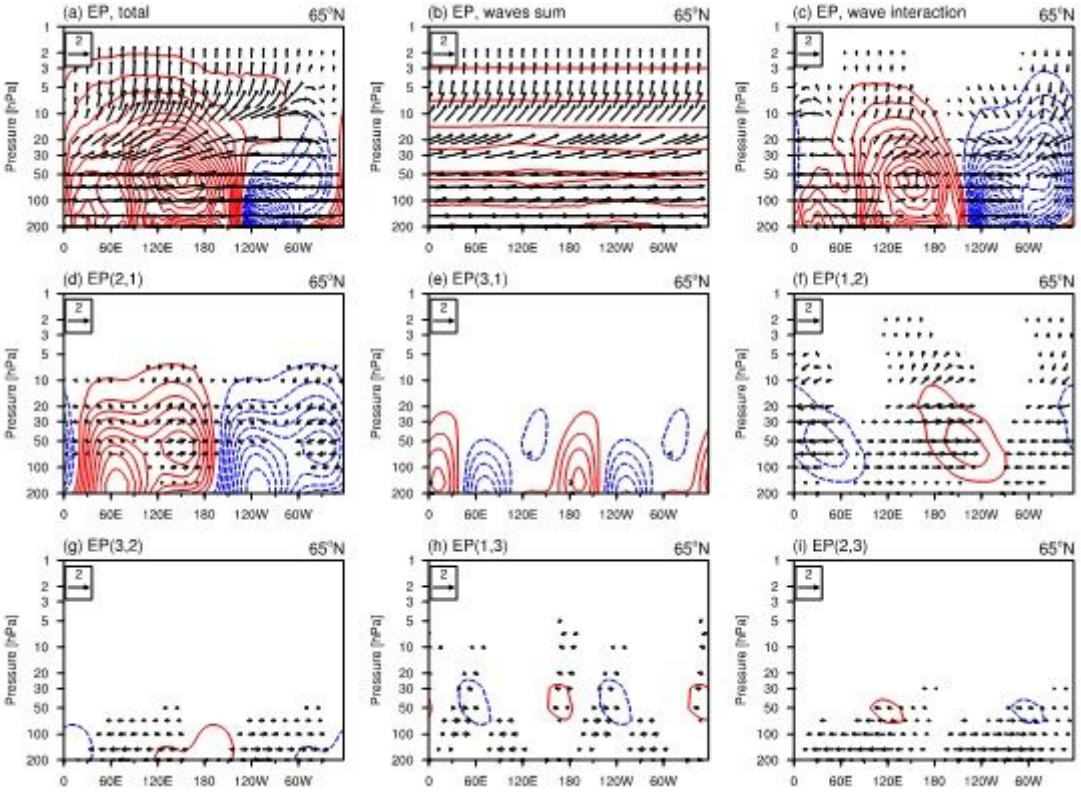

Figure 4

The winter (DJF) EP flux climatology at 65 °N for the longitude-height section: (a) total wave flux, (b) the sum of flux caused by the individual waves, (c) the total wave flux caused by the wave-wave interaction, (d) the flux caused by wave 2 acting on wave 1 (EP (2, 1)), (e) wave 3 acting on wave 1 (EP (3, 1)), (f) wave 1 acting on wave 2 (EP (1, 2)), (g) wave 3 acting on wave 2 (EP(3, 2)), (h) wave 1 acting on wave 3 (EP (1, 3)), and (i) wave 2 acting on wave 3 (EP(2, 3)). The contours are the vertical component of the EP flux (unit: m2 s-2) with an interval of 0.002 m2 s-2, and the vectors are the zonal and vertical components. The scales for the horizontal fluxes are 2 m2 s-2, as shown in the insets. The vertical component of the vectors is scaled by the inverse of the air density.

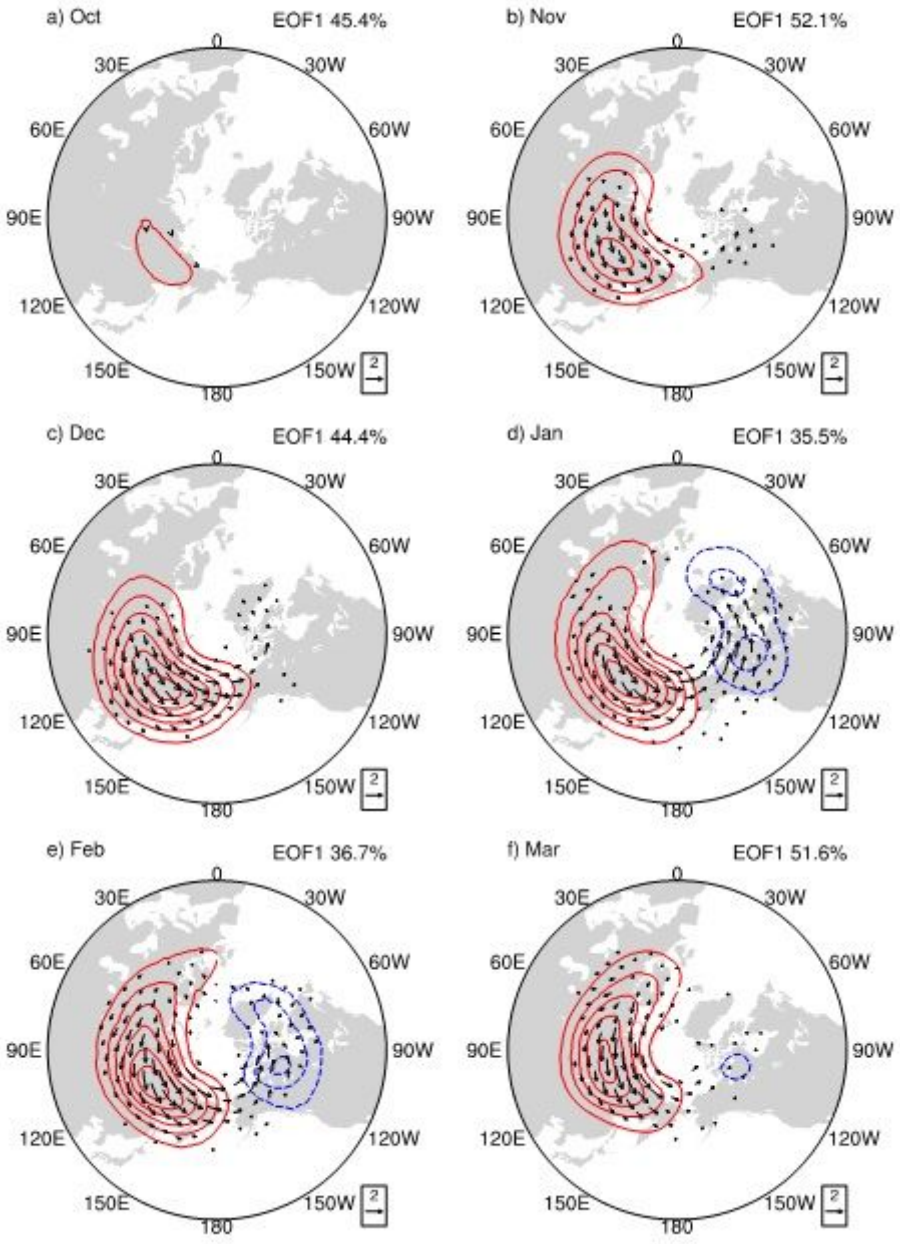

Figure 5

The first EOF of the EPz at 30 hPa expressed as regressions with their corresponding principal component (PC). Top panels: October and November; mid panels: December and January; bottom panels: February and March. Their contributions to the total variance are shown in the upper-right. The contours are the vertical component of the EP flux (unit: m2 s-2) with an interval of 0.002 m2 s-2, and the vectors are the horizontal component. The scales for the horizontal fluxes are 2 m2 s-2, as shown in the insets.Note: The designations employed and the presentation of the material on this map do not imply the expression of any opinion whatsoever on the part of Research Square concerning the legal status of any country, territory, city or area or of its authorities, or concerning the delimitation of its frontiers or boundaries. This map has been provided by the authors.

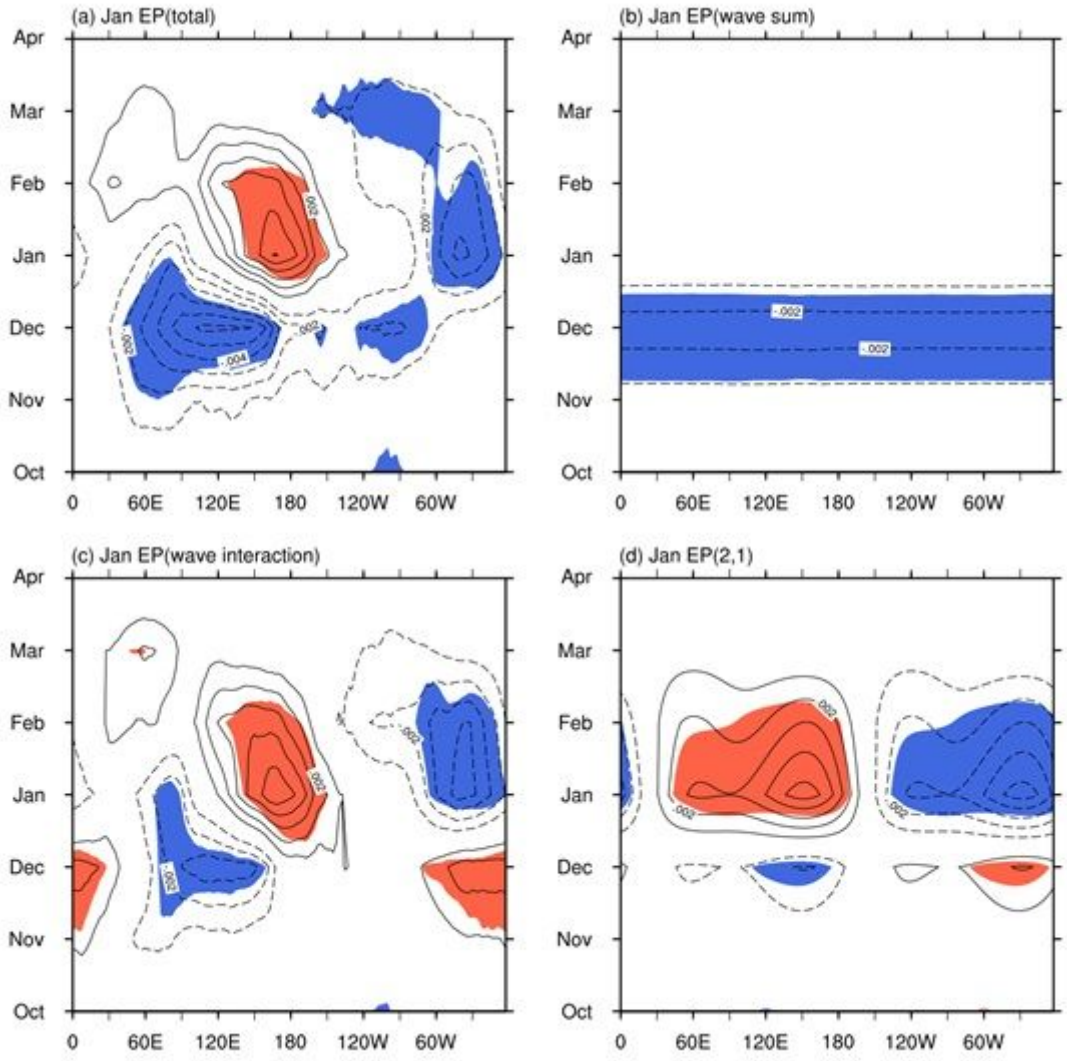

Figure 6

Hovmueller plot of the regression coefficient (contours) between (a) EPz at 30 hPa 65°N, (b) the EPz sum of wave activities from each wavenumber, (c) EPz from the interaction between waves, and (d) EPz from the action of wavenumber 2 on wavenumber 1 from October to April and the SPV index (zonal mean zonal wind at 65°N, 30 hPa) in January. Shadings indicate the region above the 95% statistically significant level.

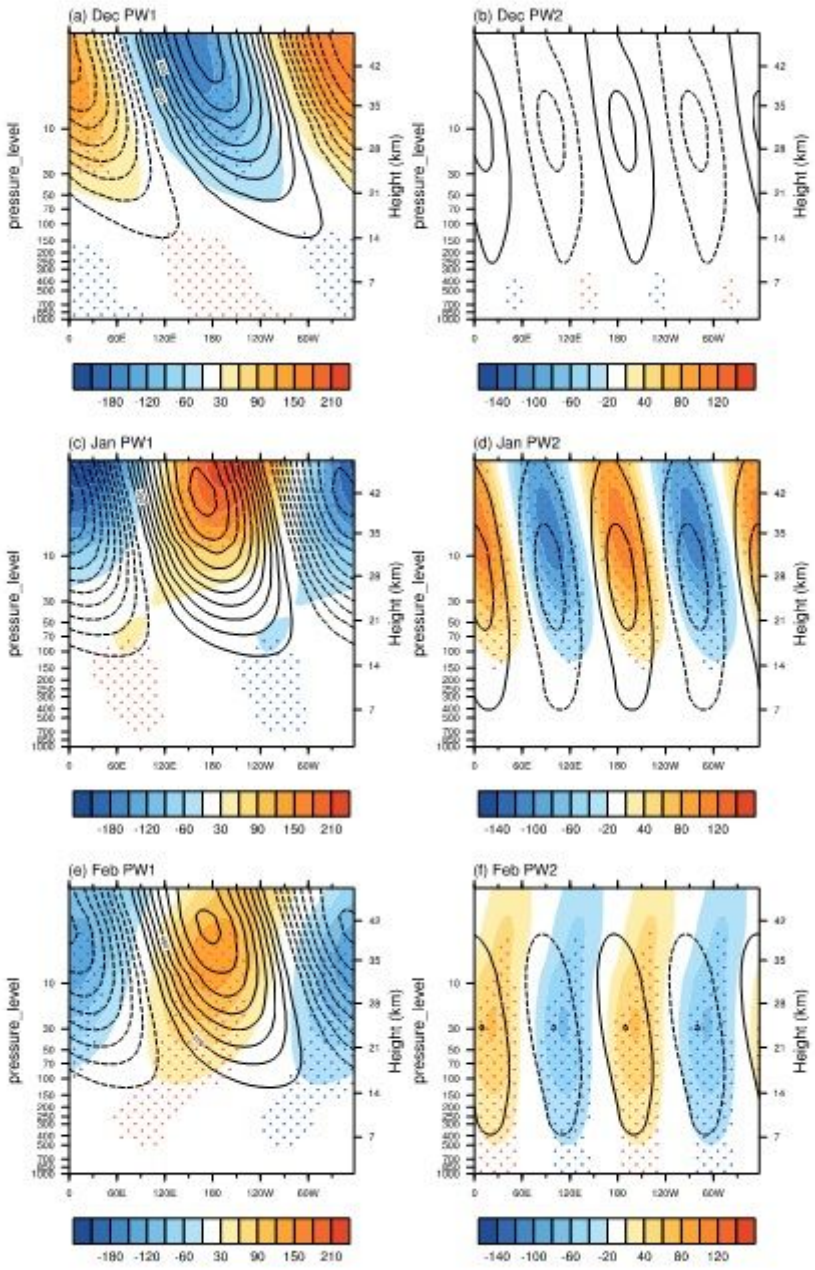

Figure 7

The regression (shading) of the wave component of geopotential in December (upper panels), January (middle panels), and February (bottom panels) on the SPV index (zonal mean zonal wind at 65°N, 30 hPa) in January. Left: wavenumber 1. Right: wavenumber 2. Contours indicate the climatology of wave component in each month, and stippling shows the significant region above the 95% confidence level.

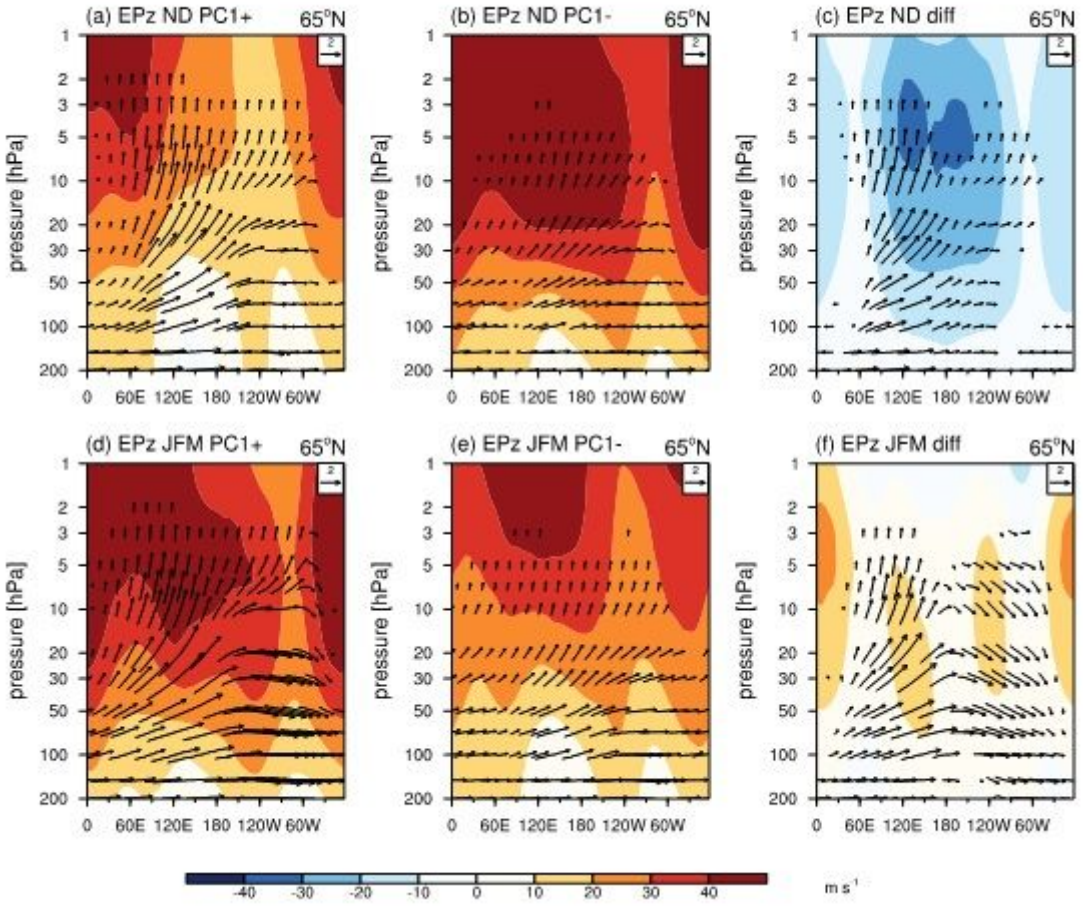

Figure 8

Longitude-height cross section of zonal wind (shading) and EP flux at 65°N composited according to the PC 1 of EPz at 30 hPa. The upper (a, b, c) panels are for the early winter of ND, and the bottom (d, e, f) panels are for the mid and late winter of JFM. (a) and (d) are composites of the positive PC1 phase, (b) and (e) are composites of the negative PC1 phase, and (c) and (f) are composite difference of the positive and negative phases, respectively.

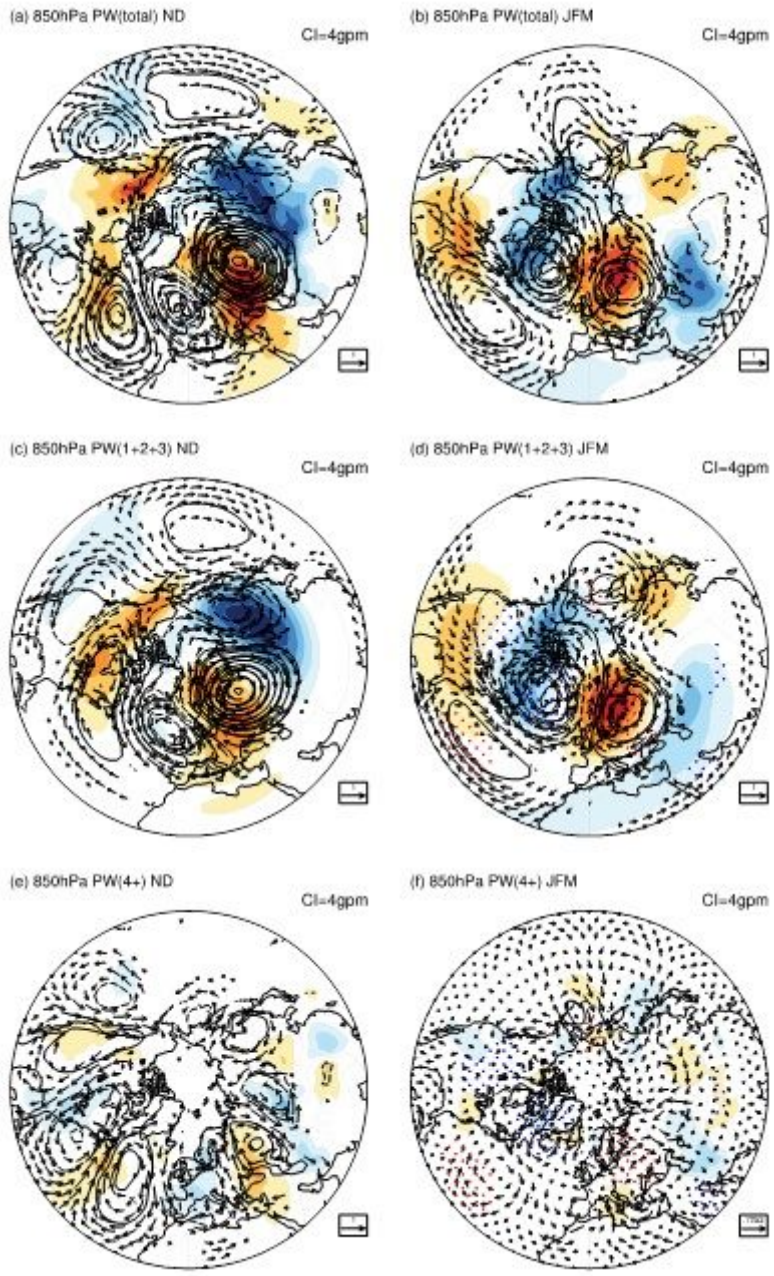

Figure 9

Regression of temperature (shadings, unit: °C), geopotential height (contours) and horizontal wind field anomalies at 850 hPa on the leading principal component of EPz EOF mode of early winter (left panels, November and December) and mid and late winter (right panels, January, February and March). (a) and (b) are for the total wave components of geopotential height (contours) and horizontal wind field, (c) and (d) for the sum of wavenumber 1, 2 and 3, and (e) and (f) for the sum of wavenumber greater than 3.
Note: The designations employed and the presentation of the material on this map do not imply the expression of any opinion whatsoever on the part of Research Square concerning the legal status of any country, territory, city or area or of its authorities, or concerning the delimitation of its frontiers or boundaries. This map has been provided by the authors.

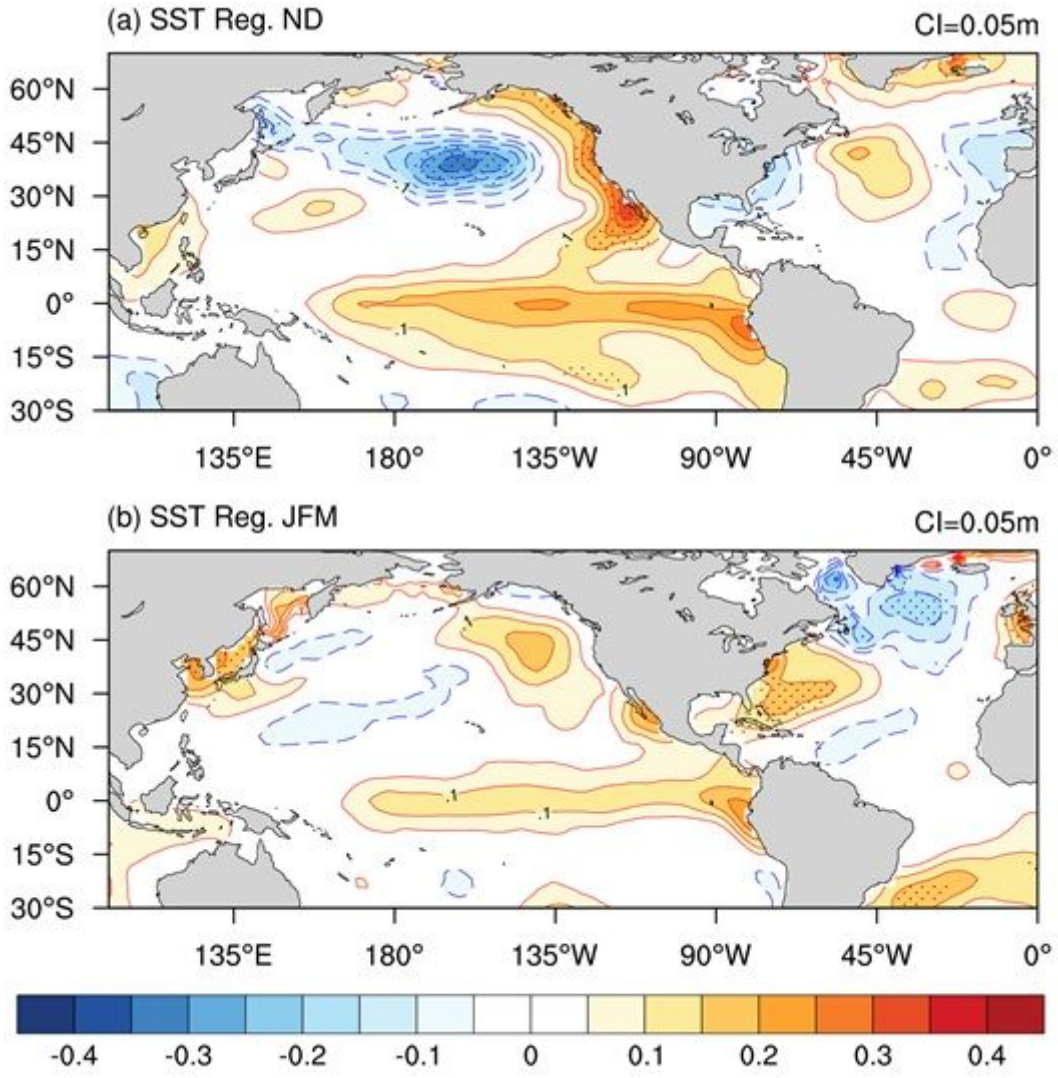

Figure 10

Regression of sea surface temperature (shadings, unit: °C) on the leading principal component of EPz EOF for (a) early winter, and (b) late winter. stippling shows the significant region above the 95% confidence level. Note: The designations employed and the presentation of the material on this map do not imply the expression of any opinion whatsoever on the part of Research Square concerning the legal status of any country, territory, city or area or of its authorities, or concerning the delimitation of its frontiers or boundaries. This map has been provided by the authors.